J. metamorphic Geol., 2007, **25,** 781–801 doi:10.1111/j.1525-1314.2007.00730.x

Clasts of Variscan high-grade rocks within Upper Viséan conglomerates – constraints on exhumation history from petrology and U-Pb chronology

J. KOTKOVÁ,[1] A. GERDES,[2,3] R. R. PARRISH[2] AND M. NOVÁK[1]
[1]*Institute of Geological Sciences, Masaryk University, Kotlářská 2, Brno, Czech Republic (kotkova@sci.muni.cz)*
[2]*NERC Isotope Geosciences Laboratory, Keyworth, Notts, NG12 5GG, UK*
[3]*Institute of Geosciences, Mineralogy, J.W. Goethe-University, Altenhoeferallee 1, 60438 Frankfurt, Germany*

ABSTRACT In this paper, U-Pb zircon, monazite and rutile data for crystalline rocks deposited as clasts in the Upper Viséan conglomerates at the eastern margin of the Bohemian Massif are reported. U-Pb data of spherical zircon from three different granulite clasts yielded a mean age of 339.0 ± 0.7 Ma ($\pm 2\sigma$), while oval and spherical grains of another granulite pebble define a slightly younger date of 337.1 ± 1.1 Ma. These ages are interpreted as dating granulite facies metamorphism. Thermochronology and the derived pressure–temperature (*P–T*) path of the granulite pebbles reflect two-stage exhumation of the granulites. Near-to-isothermal decompression from at least 44 km to mid-crustal depths of around 22 km was followed by a near-isobaric cooling stage based on reaction textures and geothermobarometry. Minimum average exhumation rate corresponds to 2.8–4.3 mm year^{-1}. The extensive medium-pressure/high-temperature overprint on granulite assemblages is dated by U-Pb in monazite at *c.* 333 Ma. This thermal event probably has a close link to generation and emplacement of voluminous Moldanubian granites, including the cordierite granite present in clasts. This granite was emplaced at mid-crustal levels at 331 ± 3 Ma (U-Pb monazite), whereas the U-Pb zircon ages record only a previous magmatic event at *c.* 378 Ma. Eclogites and garnet peridotites normally associated with high-pressure granulites are absent in the clasts but exotic subvolcanic and volcanic members of the ultrapotassic igneous rock series (durbachites) of the Bohemian Massif have been found in the clasts. It is therefore assumed that the clasts deposited in the Upper Viséan conglomerates sampled a structurally higher tectonic unit than the one that corresponds to the present denudation level of the Moldanubicum of the Bohemian Massif. The strong medium-temperature overprint on granulites dated at *c.* 333 Ma is attributed to the relatively small size of the entirely eroded bodies compared with the presently exposed granulites.

Key words: Bohemian Massif; conglomerate; granulite; monazite; U-Pb dating; Variscan flysh; zircon.

INTRODUCTION

Clasts of crystalline rocks removed by erosion from the top of a structural sequence and deposited in synorogenic sediments can provide unique material for unravelling orogenic evolution. Such material has been found within the Viséan (Lower Carboniferous) conglomerates of the Variscan flysch to molasse deposits (Culm) at the eastern margin of the Bohemian Massif. Pebbles were derived from a variety of magmatic, metamorphic and sedimentary rocks (e.g. Štelcl, 1960) including various types of granulites. The latter contain mineral assemblages that are unusual at the present erosional level. These high-grade rocks can therefore serve as clues to Variscan exhumation tectonics, using the *P–T* conditions of their maximum burial, their timing, the exhumation-related *P–T* paths and the age of their exposure at the surface, deduced from the age of conglomerate deposition.

The Variscan Belt of Central Europe is characterized by exposure of high-pressure (HP), predominantly felsic granulites along with abundant medium-pressure (MP) to low-pressure (LP) migmatites and granites. Pin & Vielzeuf (1983) noted the spatial association of the HP granulites with eclogites and garnet peridotites and distinguished them from the younger, Late Variscan MP to LP granulites. Recent studies have shown that the felsic granulites preserve the HP assemblage K-feldspar (mesoperthite)-garnet-kyanite-quartz (e.g. Carswell & O'Brien, 1993) that formed at conditions above 900 °C and in excess of 13–15 kbar. Subordinate mafic granulites (Grt-Cpx-bearing) experienced comparably high *P–T* conditions; orthopyroxene formed as a secondary phase upon their decompression (e.g. O'Brien & Rötzler, 2003). These HP rocks were formed during the Early Variscan tectonometamorphic event which involved significant crustal thickening and/or subduction of crustal material into the mantle (Carswell & O'Brien, 1993; Schulmann *et al.*, 2005). The timing of this event in the Bohemian Massif – the easternmost of the Variscan massifs in Europe – is well constrained to *c.* 340 Ma, based on numerous

© 2007 Blackwell Publishing Ltd

geochronological studies (O'Brien & Rötzler, 2003). Abundant exposures of the HP granulites in the European Variscides highlight their regional tectonic importance in the continent–continent collisional orogen (Pin & Vielzeuf, 1983; O'Brien & Rötzler, 2003).

In the Moldanubian Zone of the Bohemian Massif, HP granulites were exhumed from depths of ~50 km to their present position on the top of the Gföhl Unit, interpreted as the uppermost part of the stacked nappe pile (Tollmann, 1982; Matte *et al.*, 1990). High exhumation rates have been postulated for HP granulites from several locations (e.g. Kröner *et al.*, 2000; Romer & Rötzler, 2001). This study brings additional information on their post-peak history before their exposure at the surface.

Mineral assemblages of granulites in pebbles indicate high-temperature equilibration at variable crustal depths. Along with reaction textures, mineral composition and zoning, this suggests that the granulites were exhumed along near-to-isothermal decompression P–T paths, followed by near-to-isobaric cooling. Combined with the geochronological data and known age of sedimentation (i.e. exposure at the surface), this provides the basis to infer the exhumation rate of the rock complexes. In this paper, U-Pb zircon, monazite and rutile ages are presented for a set of crystalline rocks from pebbles, and the implications for the evolution of the eastern margin of the Bohemian Massif during the final stages of the Variscan orogeny are discussed.

GEOLOGICAL BACKGROUND

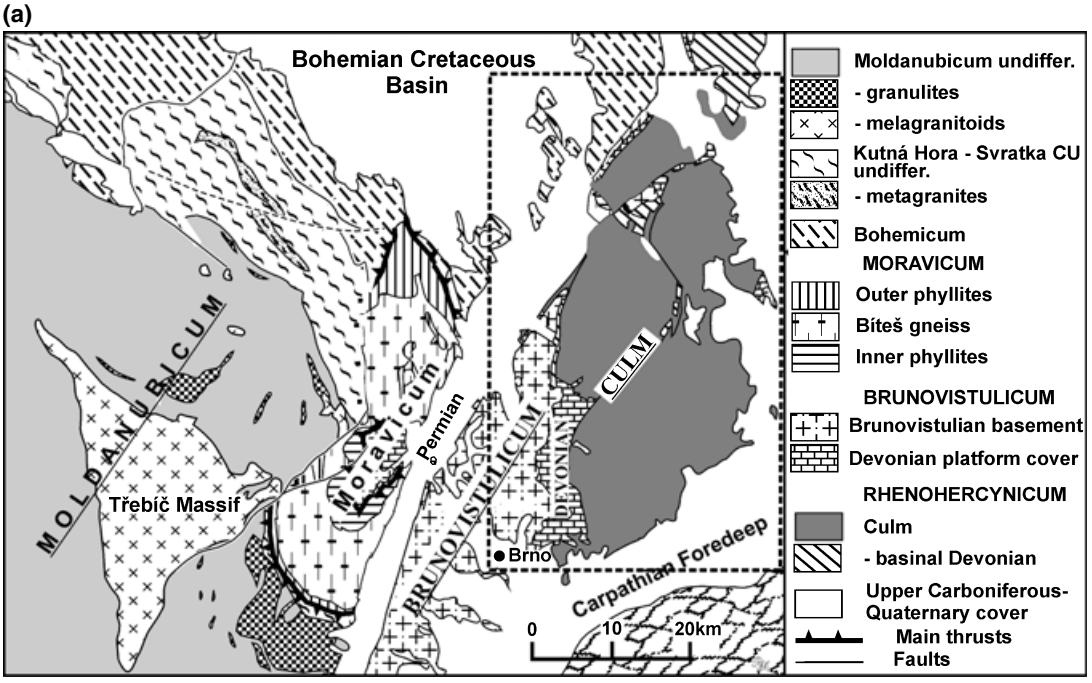
The synorogenic Viséan clastic sediments – the so-called Culm flysch (Fig. 1a) – make up part of the Moravian-Silesian Zone at the eastern margin of the Bohemian Massif. They were deposited in the NNE–SSW-trending Lower Carboniferous Culm basin, belonging to the Variscan foreland basin system (Rheno-Hercynian Zone; Franke, 1995; Bábek *et al.*, 2006). They represent an allochthonous Variscan accretionary prism, overlying Cadomian Brunovistulicum (paraautochthon) with its Devonian cover. The larger area has a complex Variscan nappe structure (Fig. 1a; see 'Tectonic scenario'), as it is actually a front of the Variscan collisional belt in contact with the Cadomian basement block (Brunovistulicum) (Dallmeyer *et al.*, 1995).

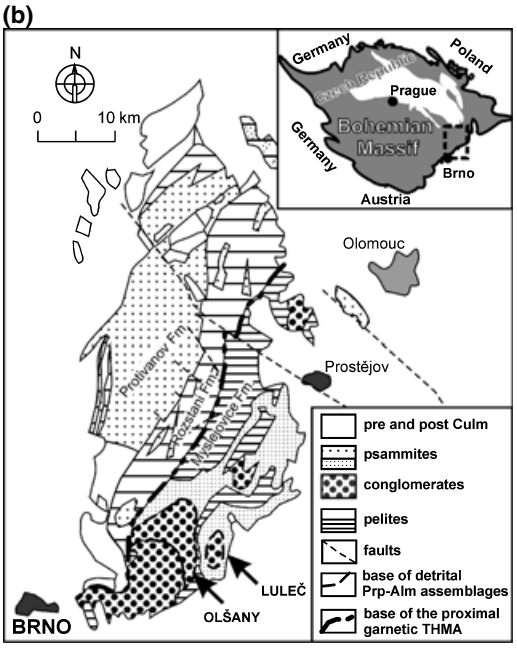
Clasts of crystalline rocks up to few metres in size can be found in the conglomerates of the final molasse unit, the so-called Myslejovice Formation (MF), in the more proximal southern part of the basin (Drahany Culm; Fig. 1b). The age of conglomerate deposition is constrained by biostratigraphy and (micro)palaeontology. The MF contains limestone pebbles with the youngest microfauna of the Middle–Upper Viséan (up to V3a) age (Špaček & Kalvoda, 2000). The index species of goniatites of all the Upper Viséan subzones (zones Goα, Goβ, Goγ), except the highest ones, were described from the shale intercalations in the upper part of this formation (Kumpera & Lang, 1975; Kumpera, 1977). $^{40}Ar/^{39}Ar$ ages of detrital muscovite from the Luleč quarry fall in the interval of 340–331 Ma (Schneider *et al.*, 1999), the younger limit of this interval correlating well with the V3a age of the limestones in pebbles (Gradstein & Ogg, 1996; Menning *et al.*, 2000). Therefore, the conglomerates, containing clasts of granulites, were deposited between 330 and 325–324 Ma, which is the base of Goγ (P2a zone) according to these time scales.

This study focuses on the clast-supported Luleč conglomerates (LC, east), occupying the uppermost position within the MF (see Fig. 1b). The clast composition changes significantly from the lowermost part of the MF–Račice conglomerates (RC, west) upward throughout the sedimentary sequence. Whereas the lowermost part of the RC is dominated by supracrustal rocks (Čopjaková & Novák, 2005; Fig. 1c), the overlying, dominant part of the RC is dominated by clasts of medium-grade metamorphic rocks (leucocratic gneisses and mica-schists with muscovite and rare garnet) and granitic rocks (Fig. 1c). The LC are dominated by metamorphic rocks (Štelcl, 1960), with characteristic presence of granulites, high-T migmatites (frequent garnet), K-Mg-rich melagranitoids (durbachites) and granites. Plutonic rocks apparently predominate over volcanic ones. The degree of anisotropy of rocks in clasts as expressed by foliation and lineation decreases gradually from the RC to the upper part of the LC (Štelcl, 1960).

Recent field studies enabled identification and detailed study of specific rock types in the LC and RC. Several types of granulites including cordierite-bearing granulites, cordierite-bearing granites, ultrapotassic igneous rocks, tourmaline-bearing granites and Fe-skarn (all exclusively in LC) are similar to related rocks from the high-grade Gföhl Unit (e.g. Kotková *et al.*, 2001; Buriánek & Novák, 2002; Zachovalová & Leichmann, 2004). This unit involves granulites, eclogites and peridotites, and makes up the uppermost part of the Moldanubian nappe sequence (Tollmann, 1982; Matte *et al.*, 1990). Graphitic quartzites containing V-muscovite, which were also found in the LC, are typical of the lower part of the Moldanubian nappe, the Drosendorf Unit (Houzar & Novák, 2001). Calcite marbles with phlogopite and garnet-tourmaline-bearing mica schists (occurring in LC, rarely in RC) have their equivalents in the lower-grade units such as Drosendorf Unit and/or Olešnice Unit attributed to the underlying Moravicum (Houzar & Novák, 2002; Čopjaková & Novák, 2003). No clasts of ultrabasic rocks (e.g. garnet peridotite) or eclogites known from the Gföhl Unit have been found, but Cr-rich spinels described from the greywacke matrix have a composition comparable with those from serpentinized peridotites common in the lower Moldanubian nappes (Čopjaková *et al.*, 2005). Some rocks found in clasts of LC such as calcalkaline andesite to rhyolite and trachyte have no equivalents in recent outcrops and may

© 2007 Blackwell Publishing Ltd





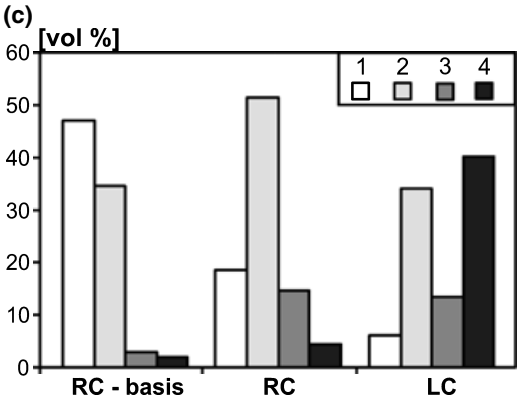




Fig. 1. (a) Tectonic map of the eastern margin of the Bohemian Massif (modified after Melichar & Kotková, 2003). (b) Lithostratigraphic map of the Drahany Culm (modified after Otava & Gilíková, 1999). Psammites and pelites of the Protivanov and Myslejovice Formation are distinguished by different line thickness. Sampled localities shown by arrows. (c) Histogram showing distribution of rock types in clasts in the Račice (RC) and Luleč conglomerates (LC). 1 – clastic sediments, contact metamorphic and volcanic rocks; 2 – phyllites, micaschists, greenschists, leucocratic muscovite and muscovite-biotite orthogneisses, metagranites; 3 – granites; 4 – biotite and cordierite-bearing rocks and granulites. Rocks grouped according to their position in the crustal section with increasing depth (according to Čopjaková & Novák, 2005). (d) Outcrop photograph showing the character of the Luleč conglomerates. Luleč quarry. Photograph by H. Gilíková.

© 2007 Blackwell Publishing Ltd

represent relics of island arcs (Zachovalová & Leichmann, 2004).

Samples with distinct mineral assemblages reflecting variable pressure conditions of their equilibration and/or later metamorphic overprint (granulites, cordierite-bearing granite) and those useful also for the provenance studies (granulites, melagranite) were selected for U-Pb age determination.

SAMPLE DESCRIPTION, *P–T* ESTIMATES AND *P–T* PATH

Granulites

A summary of the main characteristics of the dated samples is given in Table 1 (samples LU4 and LU6 are those described by Vrána & Novák, 2000). Mineral assemblages and fabrics of the rocks are shown in Figs 2–4. Mineral abbreviations are from Kretz (1983) except for: dumortierite (Dum), monazite (Mz) and xenotime (Xt). Representative mineral analyses are given in Table 2. Felsic garnetiferous granulites of leucogranitic (LU6) to granodioritic composition (LUA20), with mineral assemblage Qtz–Kfs (mesoperthite)–Grt ± Pl ± Sil (Figs 2a,c & 4a,b), represent the most abundant granulite type found in clasts. Aluminosilicate is absent or rare, present in the form of oriented prismatic sillimanite as well as large grains of sillimanite possibly replacing former kyanite (LUA20). Highly peraluminous garnet-cordierite-prismatic sillimanite-bearing granulite of metasedimentary character is much rarer (LUA3; Fig. 2b). In this sample, garnet is extensively consumed by a complex symplectite dominated by cordierite and orthopyroxene (Kotková *et al.*, 2001; Figs 2b & 4c), and sillimanite is locally replaced by hercynitic spinel and plagioclase. Garnet-orthopyroxene-bearing intermediate granulite (LUA28; Fig. 2d) and biotite-garnet granulite (LU4; Fig. 2f) with paragneiss-like composition and grossular-rich garnet represent other rare granulite types. All the samples are massive, and only LUA3 is banded (millimetre-thick bands rich in biotite) and has preferred orientation of sillimanite and late biotite (Fig. 2b) in an otherwise undeformed (dynamically recrystallized) matrix.

Granulites from pebbles differ from those cropping out in the Moldanubian granulite massifs by the presence of the highly peraluminous varieties. Other contrasting features are the scarcity of aluminosilicates in the felsic rock clasts and the extensive HT/MP overprint reflected by low grossular content in garnet, lack of garnet zoning and occurrence of Crd-Opx symplectite on garnet.

As a result of this overprint, the peak pressures of the rock burial and the peak temperatures are difficult to be retrieved. The biotite-garnet granulite (LU4) that is much less overprinted at MP is not helpful in this respect because of its restricted mineral assemblage. Nevertheless, minimum peak pressure can be derived using the higher grossular (Grs) values preserved in cores of large garnet ($Alm_{50}Prp_{43}Grs_6$) and plagioclase core composition (An32; sample LUA20, see Table 1 and Fig. 4). This pressure value was estimated to be ~12 kbar using the GASP barometer (calibration of Newton & Haselton, 1981) for a minimum temperature of 820 °C (two-feldspar thermometry using Ca-rich plagioclase cores and bulk composition of fine perthite cores; Fuhrman & Lindsley, 1988). These conditions are consistent with the original stability of kyanite later pseudomorphosed by sillimanite. Calcium decrease at garnet rim suggests a significant decompression by about 4 kbar, as determined by GASP barometry, using garnet rim and plagioclase rim compositions (Fig. 5).

Low Ca values encountered at garnet rims or throughout the garnet grains and the coexistence of Mg-cordierite and orthopyroxene in the symplectites (Fig. 4c) probably reflect an extensive MP overprint on the HP granulite assemblages at temperatures in excess of 800 °C. The *P–T* conditions of this stage have been estimated to be ~6 ± 1 kbar and ~820 °C (average *T*, TWQ 2.02, Berman, 1991; non-ideal activity model of garnet according to Berman & Aranovich, 1996), using the Grt rim ($Alm_{67}Prp_{27}Grs_3$)-Crd ($X_{Mg} = 0.76$)-Opx ($X_{Mg} = 0.55$, $X_{Al} = 0.244$)-Sil assemblage in sample LUA3, assuming that domainal equilibrium has been approached. This is suggested by the uniform garnet rim

Table 1. Mineral assemblages and whole-rock composition of the dated samples (based on modal and unpublished bulk-rock data).

Sample no.	Locality	Rock type	Whole-rock composition	Mineral assemblage	Accessory phases
LUA20	Luleč	Garnet-rich granulite	Granodioritic	Grt-Ky/Sil-Qtz-Kfs-Pl-Bt $Alm_{50-53}Prp_{43-46}Grs_{3-6}$	Zrn, Mz, Rt
LUA3	Luleč	Grt-Crd-Sil granulite	Intermediate	Grt-Sil-Qtz-Kfs > Pl-Crd-Opx-Spl-Bt $Alm_{48}Prp_{48}Grs_3$	Zrn, Mz, Rt
LUA28	Luleč	Grt-Opx granulite	Granodioritic to tonalitic	Grt-Bt-Opx-Qtz-Kfs-Pl (Crd) $Alm_{60-65}Prp_{23-27}Grs_{6-12}$	Zrn, Rt
LU6	Luleč	Garnet leucogranulite	Leucogranitic	Grt-Qtz-Kfs > Pl $Alm_{70}Prp_{27-29}Grs_{1-3}$	Zrn, Rt
LU4	Luleč	Biotite-garnet granulite	Paragneiss-like	Grt-Bt-Qtz-Kfs-Pl $Alm_{48-56}Prp_{32}Grs_{25-12}$	Zrn, Rt
LUA2	Luleč	Cordierite granite	S-type granite	Qtz-Kfs-Pl-Bt-Crd-Grt (Ms) $Alm_{83}Prp_{10}Grs_2Sps_5$	Ap, Zrn, Mz, Xt, Rt Ilm, Dum
B2	Olšany	Durbachite	Melagranite	Qtz-Kfs-Pl-Bt (Hbl)	Ap, Zrn, Mz, Rt

© 2007 Blackwell Publishing Ltd

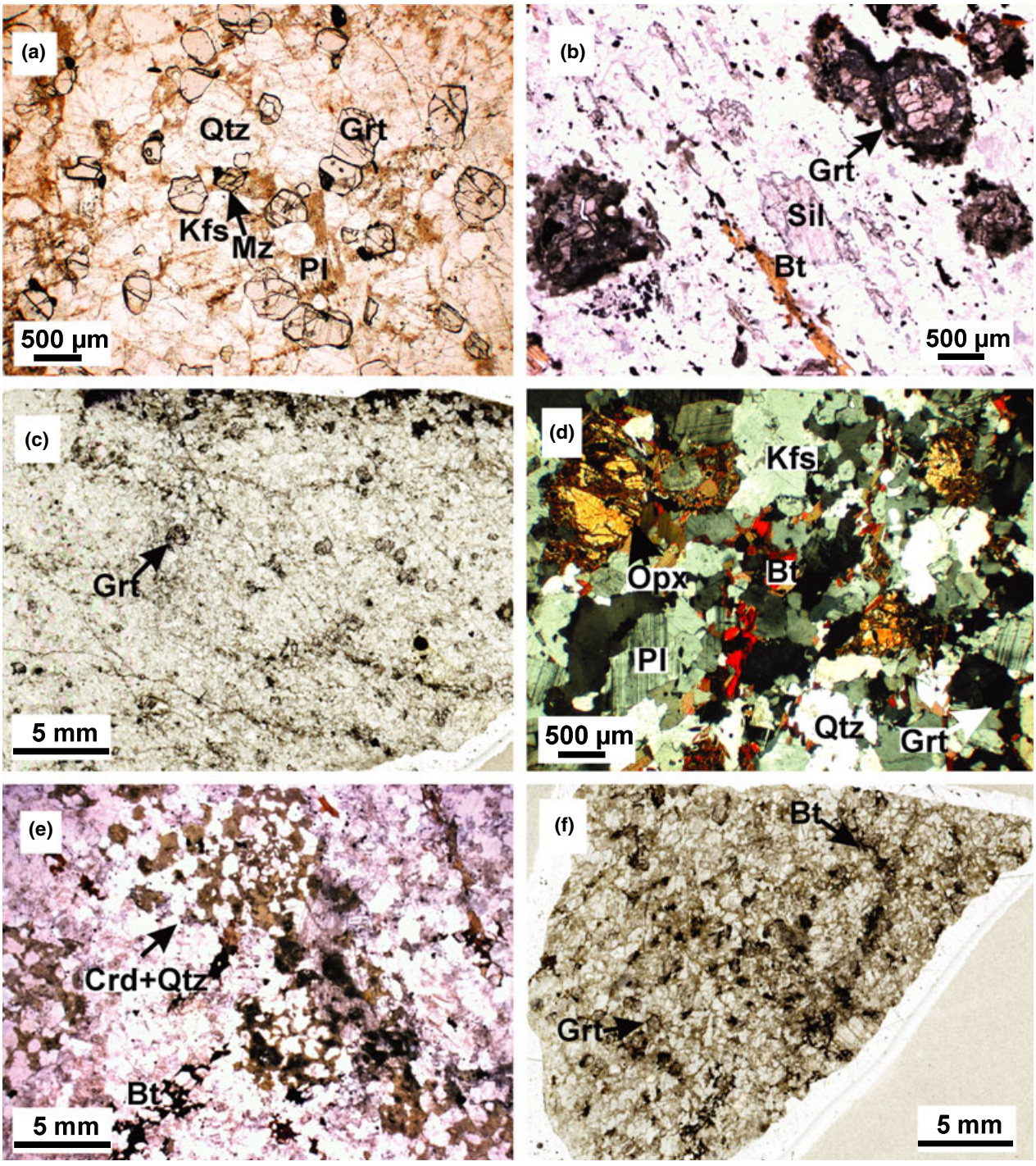


Fig. 2. Photomicrographs of dated rocks showing their fabrics and mineral assemblages. (a) garnet-rich granulite LUA20; (b) Grt-Crd-Sil granulite LUA3; (c) garnet leucogranulite LU6; (d) Grt-Opx granulite LUA28 (crossed polarized light); (e) cordierite granite LUA2; (f) biotite-garnet granulite LU4.

composition. Fe/Fe + Mg of 0.71 at the garnet rim corresponds well to the 0.7 isopleth for the assemblage Grt-Opx-Crd-Qtz (Spear, 1993, p. 389) at the calculated *P–T* conditions. Fe/Fe + Mg decreases to 0.47 in the garnet core (indicating higher pressures) and suggests that the rock experienced decompression of at least ~3–4 kbar (Fig. 5). Biotite ± muscovite and chlorite formed at the expense of garnet during successive cooling of the rocks.

Orthopyroxene-bearing granulite reflects MP (re-) equilibration at pressures of 7 ± 1 kbar (Al-in-Opx –

© 2007 Blackwell Publishing Ltd

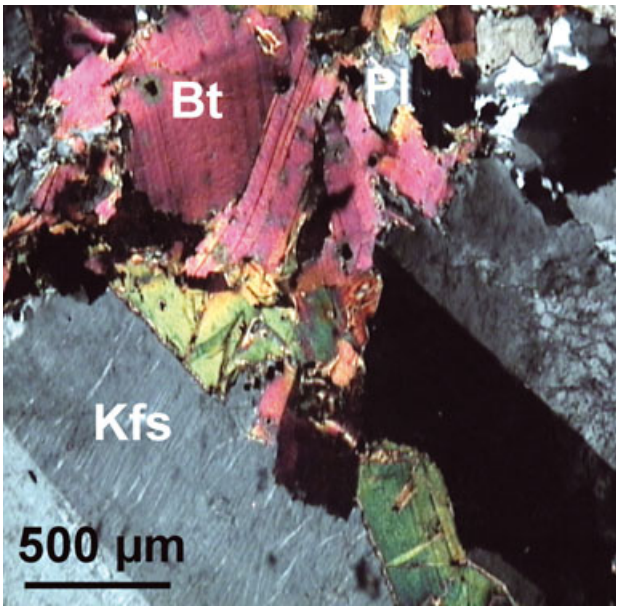


Fig. 3. Photomicrograph of melagranite B2.

Harley, 1984a; garnet-plagioclase-orthopyroxene-quartz – Newton & Perkins, 1982; Bohlen *et al.*, 1983, cores) for 750 °C (Grt-Opx, Harley, 1984b, cores). Representative core mineral compositions are $Alm_{63}Grs_8Prp_{28}$, Opx – $X_{Mg} = 0.52$, $X_{Al} = 0.09$, Pl – $X_{An} = 0.35$. Mineral zoning towards the rim of several phases – Grs ± Prp decrease in garnet, Al_2O_3 and CaO decrease in Opx ($X_{En} = 52$–54) and anorthite increase in plagioclase – is consistent with further pressure and temperature decrease. Broad homogeneous cores of Grt may reflect an extensive diffusional reequilibration resulting in obliteration of any possible evidence of higher-grade conditions.

Observed mineral reactions, mineral zoning and *P–T* estimates of two to three granulite samples (felsic garnetiferous granulite LUA20, strongly peraluminous granulite LUA3 and to a certain extent Grt-Opx-bearing granulite LUA28) are comparable and suggest the two-stage evolution of the rocks (Kotková *et al.*, 2002). The first stage corresponds to the near-to-isothermal decompressional exhumation of the granulites by at least 15 km from minimum depths of 44 km

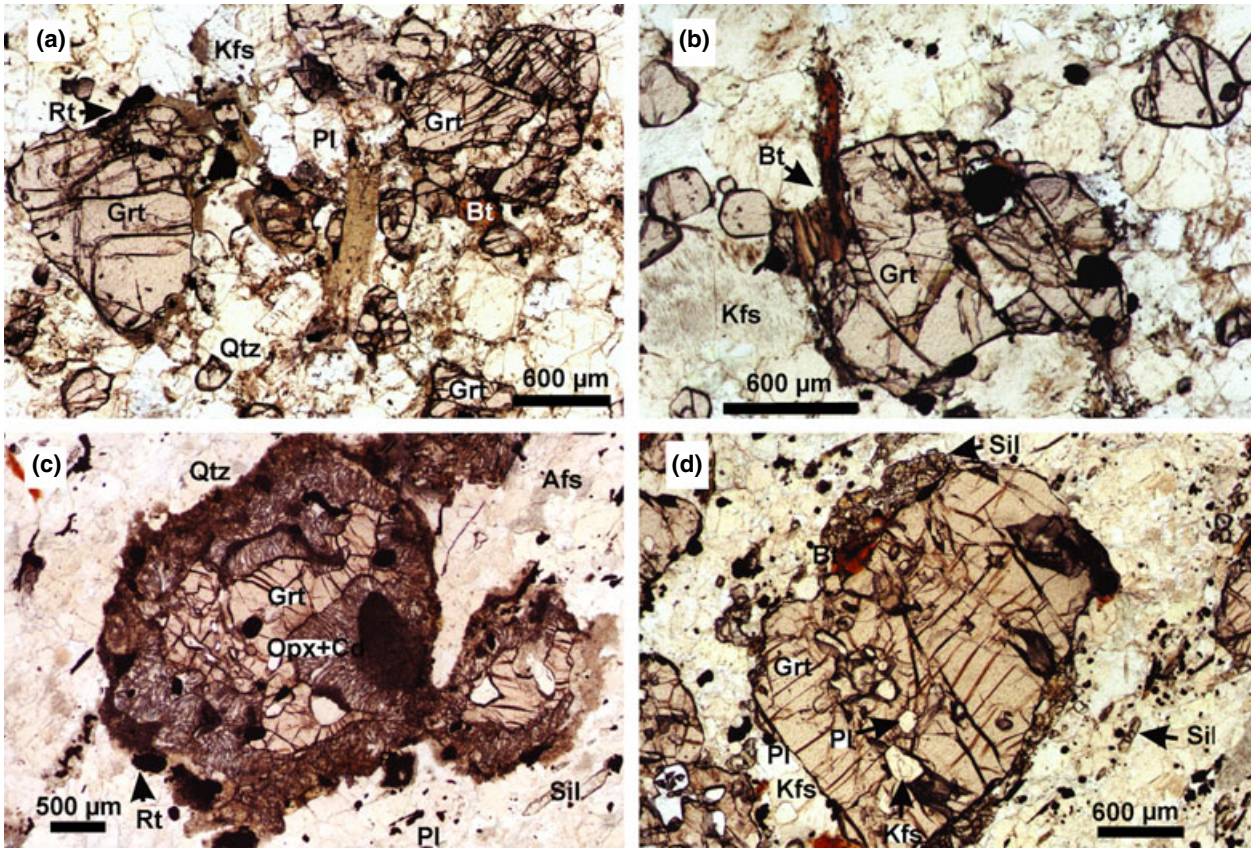


Fig. 4. Photomicrographs showing mineral assemblages and reaction textures which served as basis for the *P-T*-path reconstruction. (a) & (b) Garnet-rich granulite LUA20. (a) large garnet analysed (left), having elevated Ca in the core; (b) biotite replacing garnet. (c) & (d) Grt-Crd-Sil granulite LUA3. (c) Crd-Opx symplectite replacing garnet, (d) mineral assemblage of the rock including oriented sillimanite grains.

© 2007 Blackwell Publishing Ltd

Table 2. Representative electron microprobe analyses of minerals from selected granulite samples.

Sample	LUA3a	LUA3a	LUA3a	LUA3a	LUA3a	LUA3a	LUA20	LUA20	LUA20	LUA20	LUA20
Mineral	Opx	Cd	Grt1	Grt1	Grt2	Grt2	Pl	Kfs	Grt	Grt	Grt
Position	symplectite	symplectite	core	rim	core	rim	core	matrix[a]	core	rim–sympl	rim
SiO_2	49.6	49.9	38.4	38.1	39.6	39.7	60.8	63.8	39.2	38.8	39.4
TiO_2	0.11	< 0.01	0.04	< 0.01	0.07	0.04	< 0.01	< 0.01	0.02	< 0.01	0.01
Al_2O_3	5.46	33.9	21.6	21.5	22.5	22.2	25.0	19.7	22.1	21.7	22.0
Cr_2O_3	0.12	n.a.	0.06	0.10	0.05	0.08	n.a.	n.a.	0.01	0.10	0.06
FeO	26.1	5.99	30.5	32.3	23.0	24.1	0.00	0.00	23.8	28.4	24.5
MnO	0.18	0.04	0.54	0.79	0.35	0.39	< 0.03	< 0.03	0.40	0.63	0.41
MgO	18.02	10.58	8.57	6.94	13.22	12.93	0.01	0.00	11.56	9.51	12.21
CaO	0.19	0.03	1.19	1.18	1.43	0.62	6.56	1.06	2.23	1.01	1.05
Na_2O	< 0.02	0.08	0.02	0.09	0.04	0.02	7.55	2.74	< 0.02	0.03	0.03
K_2O	0.01	0.01	n.a.	n.a.	n.a.	n.a.	0.55	11.81	n.a.	n.a.	n.a.
Total	99.9	100.5	100.9	101.0	100.2	100.0	100.5	99.1	99.3	100.0	99.6
No. oxygen	6	18	24	24	24	24	32	32	24	24	24
Si	1.89	4.97	5.91	5.91	5.92	5.97	10.77	11.75	5.96	5.97	5.97
Ti	0.00	0.00	0.00	0.00	0.01	0.00	0.00	0.00	0.00	0.00	0.00
Cr	0.00		0.01	0.01	0.01	0.01	0.00	0.00	0.00	0.01	0.01
Al	0.24	3.98	3.92	3.94	3.96	3.93	5.22	4.27	3.97	3.93	3.93
Fe^{3+}	0.00	0.00	0.25	0.24	0.18	0.10	0.00	0.00	0.00	0.00	0.00
Fe^{2+}	0.83	0.50	3.67	3.97	2.70	2.93	0.00	0.00	3.03	3.66	3.11
Mn	0.01	0.00	0.07	0.10	0.05	0.05	0.00	0.00	0.05	0.08	0.05
Mg	1.02	1.57	1.97	1.61	2.95	2.90	0.00	0.00	2.62	2.18	2.76
Ca	0.01	0.00	0.20	0.20	0.23	0.10	1.25	0.21	0.36	0.17	0.17
Na	0.00	0.02	0.01	0.03	0.01	0.01	2.60	0.98	0.00	0.01	0.01
K	0.00	0.00	0.00	0.00	0.00	0.00	0.12	2.77	0.00	0.00	0.00
Sum	4.00	11.04	16.00	16.00	16.00	16.00	19.97	19.98	16.00	16.00	16.00
X_{Mg}	0.55	0.76									
Fe/Fe + Mg			0.65	0.71	0.48	0.50					
Alm			0.54	0.68	0.46	0.39			0.49	0.59	0.50
Grs			0.00	0.00	0.00	0.00			0.06	0.03	0.03
Prp			0.41	0.27	0.50	0.58			0.44	0.37	0.47
Sps			0.02	0.02	0.01	0.01			0.01	0.01	0.01
Ab							0.66	0.25			
An							0.31	0.05			
Or							0.03	0.70			

[a]Beam diameter 20 μm.
n.a., not analysed.

(~12 kbar and average crustal density of 2.8 g cm^{-3}) and the MP overprint at depths of about 22 km (~6 kbar). The second stage was dominated by near-to-isobaric cooling (Fig. 5).

Magmatic rocks

Cordierite-bearing granite with the mineral assemblage Qtz-Kfs-Pl-Bt-Crd-Grt (± Ms) is strongly peraluminous. K-feldspar is perthitic and plagioclase has an X_{An} of 0.16–0.27. The rock texture is characterized by several centimetre-long linear aggregates of up to 4 mm large biotite crystals (Ti-rich; $X_{Mg} = 0.35$–0.37) and up to 1.5 cm large rounded patches of cordierite ($X_{Mg} = 0.50$–0.62) intergrown with quartz (Fig. 2e). Cordierite is partly replaced by a second textural generation of biotite (biotite II) and muscovite and successively by fine-grained chlorite. The rock texture and mineral composition suggest formation of cordierite and quartz aggregates through a reaction involving biotite and melt at moderate pressures (Barbey *et al.*, 1999).

Sample B2 (Olšany quarry; Fig. 1b) is a K-Mg-rich porphyritic melagranite, with a mineral assemblage of Qtz-Kfs-Pl-Bt (Hbl), rich in biotite and euhedral to subhedral K-feldspar phenocrysts (≤3 cm; Fig. 3). Its bulk-rock composition corresponds to the leucocratic members of the ultrapotassic igneous rock series of the Bohemian Massif (Holub, 1997). Both feldspars exhibit distinct oscillatory zoning. The coarse-grained matrix has a granodioritic character. Apatite as acicular inclusions in biotite is the most common accessory mineral. Oscillatory-zoned zircon and unzoned monazite are common inclusions in biotite and plagioclase.

ANALYTICAL TECHNIQUES

Samples (Table 1) were processed for U-Pb geochronology at the NERC Isotope Geosciences Laboratory (NIGL) in the UK using standard mineral separation techniques. All zircon fractions were abraded 2–8 h with the air abrasion technique of Krogh (1982) to remove rims of questionable origin. Zircon, monazite and rutile fractions were spiked with a mixed $^{205}Pb/^{233}U/^{235}U/^{230}Th$ tracer. Dissolution of zircon fractions was performed in Parr@ bombs (Parrish, 1987) in a 4:1 HF:HNO_3 mixture over 120 h at 240 °C. Monazite was dissolved in a similar way but using 12 M HCl and a temperature of only 180 °C. Complete

© 2007 Blackwell Publishing Ltd

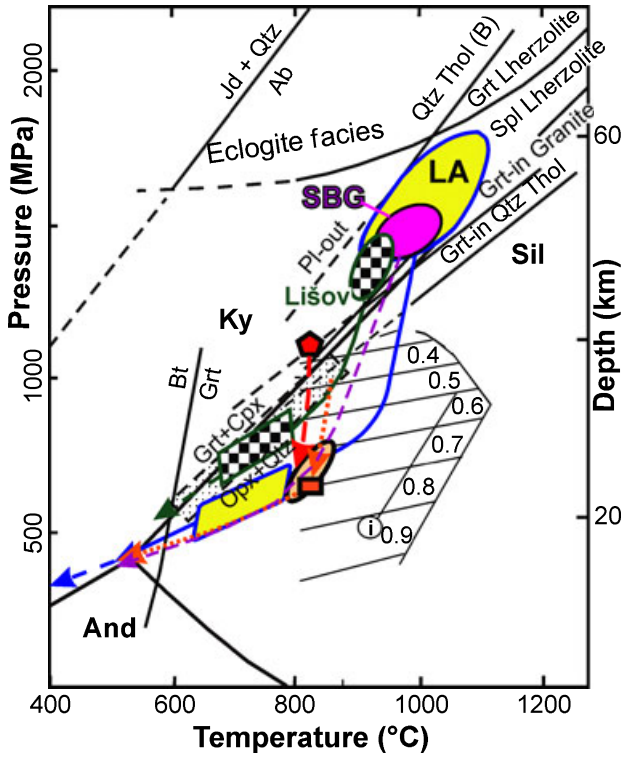


Fig. 5. *P–T* path of the granulite clasts. Pentagon – garnet-rich granulite LUA20, ellipse – garnet-orthopyroxene granulite LUA28, rectangle – garnet-cordierite-sillimanite granulite LUA3. Isopleths are contours of Fe/Fe+Mg in garnet for the assemblage Grt-Opx-Crd-Qtz, reaction i – Grt + Crd + Sil = Spl + Qtz (both from Spear, 1993). Dashed and dash-dot steep lines correspond to decompression derived from Ca, respectively Fe/Fe+Mg zoning in garnet (our samples). *P-T* fields and *P-T* paths of granulites from the Lower Austria (LA; Carswell & O'Brien, 1993), granulites of the South Bohemian Moldanubicum (SBG; Vrána, 1992; Kotková & Harley, 1999) and of the Lišov granulite massif (Kotková, 1998a,b) are shown, too. Position of reactions – references: Ab = Jd + Qtz (Holland, 1980); Grt- in and Pl-out for quartz tholeiites and Grt + Cpx = Opx + Pl (Green & Ringwood, 1967); Grt-in for granite compositions (Green & Lambert, 1965); garnet lherzolite = spinel lherzolite (O'Hara *et al.*, 1971).

dissolution was checked under the microscope before evaporation, re-dissolution and subsequent chemical purification of the U-Pb fraction with micro-anion exchange columns (Parrish, 1987). Isotope data were obtained by analytical procedures described in Noble *et al.* (1993) with a VG354 mass spectrometer fitted with a WARP filter and ion-counting Daly detector. A multiple Faraday cup collection was used for the larger ion beams. Pb isotope ratios were corrected for initial common Pb in excess of laboratory blank using the common Pb evolution model of Stacey & Kramers (1975). Laboratory blanks during the period of analysis were below 10 pg.

Errors were calculated by numerical error propagation taking all uncertainties into account (Roddick, 1987). Analytical data are presented in Table 3. Discordias were calculated using a modified York (1969) regression and isotope ratios are plotted in Figs 6 and 7 using ISOPLOT (Ludwig, 1989, 2001), with error ellipses reflecting 2σ (95% confidence level) uncertainty.

Polished grain mounts for cathodoluminescence (CL) and backscatter electron imaging (BSE) were made to detect zoning and multiple growth zones, e.g. cores, within zircon. Zircon grains were embedded in epoxy resin (Epofix) and, after hardening, were ground and polished. The CL images were produced with a desktop CL facility attached to a polarization microscope at Leicester University and a JEOL JXA-8900 electron microprobe at Frankfurt University; backscatter images were produced with a Hitachi S500 scanning electron microscope with a Link AN10000 energy-dispersive X-ray analysis system (EDS) at Leicester University. The BSE images of the accessory phases in thin section were prepared using a CAMECA microprobe SX 100 equipped with EDS KEVEX Delta of 80–135 eV sensitivity and ultra-thin window MOXTEK AP 1.3 at GUDS Bratislava, Slovakia, and CAMECA microprobe SX 50 at Ruhr-Universität Bochum, Germany. This technique enabled the study of textural relationships as well as the internal structure of zircon and monazite grains.

ACCESSORY MINERALS

Zircon

Zircon from the granulite samples is of two main types (Table 3; Figs 6 & 7). More or less spherical grains are omnipresent, which are multifaceted to sub-rounded, often somewhat irregular and clear to very cloudy. The granodioritic garnet-rich granulite (LUA20) and strongly peraluminous Grt-Crd-Sil-bearing granulite (LUA3) contain only large zircon (200–300 μm in diameter) of this type. The other samples contain in addition long to short prismatic, and in some cases oval and composite (LUA28), grains.

The spherical grains are typical for granulites of the Bohemian Massif (e.g. Kotková *et al.*, 1996; Kröner *et al.*, 2000) and are generally explained as grown or recrystallized during granulite facies metamorphism (Pidgeon, 1992). The zircons in this study show relatively homogeneous internal texture; some have a core with low luminescence, surrounded by an intermediate mantle and a bright rim of only ~5–10 μm width (e.g. Fig. 6a,c), others have instead a core with bright luminescence (Fig. 5b) or show no variation from core to rim (Fig. 5g).

Long to short prismatic zircon are variably rounded, commonly with similar internal textures as spherical grains, e.g. homogeneous (Zrn13; Fig. 6h) or with dark core, intermediate mantle and light rim (Fig. 6c,d). Other grains show sector zoning or relict oscillatory zoning in the inner parts (Fig. 6e; and Zrn11 in Fig. 6h,i), typical for magmatic zircon (Corfu *et al.*, 2003).

© 2007 Blackwell Publishing Ltd

Table 3. U-Pb zircon, monazite and rutile data for the dated samples.

	Concentrations					Atomic ratios						Age $\pm 2\sigma$ (Ma)					
Sample, fraction[a]	Wt[b] (μg)	U (ppm)	Pb[c] (ppm)	Pb[d] (pg)	Th/U	$^{206}Pb/^{204}Pb$[e]	$^{206}Pb/^{238}U$[f]	$\pm 1\sigma$ (%)	$^{207}Pb/^{235}U$[f]	$\pm 1\sigma$ (%)	Rho	$^{207}Pb/^{206}Pb$[f]	$\pm 1\sigma$ (%)	$^{206}Pb/^{238}U$	$^{207}Pb/^{235}U$	$^{207}Pb/^{206}Pb$	Disc.[g] (%)
LUA20 Garnet-bearing felsic granulite																	
Zrn1 -s, rm, 200 × 200, cl	33	353	17.7	20.7	0.06	9739	0.05405	0.34	0.3996	0.39	0.93	0.0536	0.15	339.3 ± 2.3	341.4 ± 2.3	355 ± 7	5.9
Zrn2 -s, rm, 200 × 200, cl	35	265	14.4	66.8	0.07	861	0.05422	0.34	0.3981	0.59	0.82	0.0533	0.37	340.4 ± 2.3	340.3 ± 3.5	340 ± 17	0.4
Zrn3 -s, rm, 200 × 200, cl	32	409	20.1	39.9	0.03	4114	0.05385	0.33	0.3965	0.42	0.88	0.0534	0.20	338.1 ± 2.2	339.1 ± 2.4	346 ± 9	3.6
Mz1 -s, sh, 200 × 200, cl	11	1944	919	71.0	28.3	2460	0.05448	0.33	0.3957	0.43	0.92	0.0527	0.18	341.9 ± 2.2	338.5 ± 2.5	315 ± 8	−7.4
Mz2 -s, sh, 100 × 100, cl	7	395	171	40.7	25.9	864	0.05382	0.35	0.3899	0.89	0.75	0.0525	0.73	338.0 ± 2.3	334.3 ± 5.1	309 ± 30	−11
Mz3 -s, eh, 250 × 150, cl	38	2196	870	104	23.5	3925	0.05379	0.35	0.3922	0.38	0.98	0.0529	0.08	337.7 ± 2.3	336.0 ± 2.2	324 ± 4	−3.4
Mz4 -s, sh, 200 × 200, cl	9	1803	918	55.7	31.2	2206	0.05368	0.33	0.3895	0.43	0.92	0.0526	0.20	337.1 ± 2.2	334.0 ± 2.5	313 ± 9	−6.8
Mz5 -s, sh, 200 × 200, cl	7	1681	1109	40.6	41.9	3772	0.05323	0.44	0.3882	0.59	0.91	0.0530	0.27	334.4 ± 3.0	333.1 ± 3.4	324 ± 12	−0.6
Rt2 -m, sh, 200–300, db	551	16.4	1.40	379	< 0.01	107	0.05278	0.40	0.3824	1.88	0.82	0.0526	1.53	331.5 ± 2.6	328.8 ± 10	309 ± 70	−15
LUA3 Garnet-bearing intermediate granulite																	
Zrn1 -s, rm, 240 × 180, cl	32	499	24.6	34.0	0.04	2897	0.05402	0.20	0.3968	0.23	0.91	0.0533	0.10	339.2 ± 1.3	339.3 ± 1.3	341 ± 4	0.4
Zrn2 -s, rm, 250 × 250, cl	43	486	23.7	24.0	0.02	14857	0.05393	0.37	0.3963	0.39	0.93	0.0533	0.14	338.6 ± 2.4	339.0 ± 2.3	341 ± 6	0.8
Mz1 -s, sh, 100 × 100, cl	5	2701	915	10.6	26.7	12064	0.05300	0.10	0.3882	0.14	0.78	0.0531	0.08	333.1 ± 0.7	333.4 ± 0.9	331 ± 4	−1.1
Rt1 -m, eh, c.100 × 60, rb	303	143	6.75	161	< 0.01	2823	0.05226	1.01	0.3835	1.08	0.96	0.0532	0.32	338.4 ± 6.5	329.6 ± 6.1	339 ± 14	3.1
Rt2 -m, eh, c.130 × 70, rb	270	97	4.67	13.4	< 0.01	25500	0.05289	0.22	0.3873	0.23	0.94	0.0531	0.08	332.2 ± 1.5	332.4 ± 1.3	334 ± 4	0.5
LUA28 Garnet-orthopyroxene-bearing granulite																	
Zrn16 -m, sp, 240 × 160, cl	31	332	18.1	50.1	0.40	1694	0.05371	0.35	0.3945	0.50	0.86	0.0533	0.27	337.3 ± 2.3	337.6 ± 2.9	340 ± 12	0.9
Zrn14 -s, rm, 280–200	28	401	20.3	8.0	0.13	23865	0.05365	0.19	0.3942	0.20	0.95	0.0533	0.06	336.9 ± 1.2	337.4 ± 1.1	341 ± 3	1.3
Zrn18 -s, o, 240 × 140, cl	11	276	13.7	9.8	0.09	5569	0.05350	0.15	0.3927	0.21	0.77	0.0532	0.14	336.0 ± 1.0	336.4 ± 1.2	339 ± 6	1.0
Zrn19 -m, co,150 × 80, cl	15	196	10.3	7.3	0.25	7123	0.05365	0.12	0.3940	0.18	0.75	0.0533	0.12	336.9 ± 0.8	337.3 ± 1.0	340 ± 5	1.0
Zrn17 -s, sp, 200 × 150, cl	14	344	21.7	88.9	0.14	292	0.05380	0.42	0.3904	1.16	0.75	0.0526	0.90	337.8 ± 2.8	334.7 ± 6.7	313 ± 41	−8.2
Zrn19 -m, co, c.150 × 100	32	198	18.0	212	0.25	187	0.05409	0.36	0.3965	1.77	0.83	0.0532	1.48	339.6 ± 2.4	339.1 ± 10	336 ± 66	−1.1
Zrn20 -m, lp/o, 150 × 100	24	91	4.8	21.7	0.09	1701	0.05396	0.35	0.3939	0.74	0.77	0.0530	0.50	338.8 ± 2.3	337.3 ± 4.3	327 ± 24	−3.8
Rt1 -m, sh, 50–350, db	227	61	2.93	41.9	0.01	1471	0.05283	0.14	0.3868	0.21	0.77	0.0531	0.14	331.9 ± 0.9	332.0 ± 1.2	333 ± 6	0.4
LU6 Garnet-bearing leucogranulite																	
Zrn11 -m, sp, 200 × 120	31	1229	57.2	96.0	0.08	1826	0.05014	0.39	0.3728	0.48	0.899	0.0539	0.22	315.4 ± 2.4	321.8 ± 2.7	368 ± 10	14.7
Zrn13 -m, sp, 150 × 100, cl	24	1104	52.2	93.2	0.07	1303	0.04850	0.35	0.3560	0.46	0.919	0.0532	0.20	305.3 ± 2.1	309.2 ± 2.5	338 ± 9	10.1
Zrn9 -s, rm, 160 × 140, cl	8	179	9.71	13.5	0.37	1982	0.05392	0.18	0.3961	0.41	0.591	0.0533	0.34	338.5 ± 1.2	338.8 ± 2.6	341 ± 15	0.6
Zrn10 -s, lp, 200 × 100	9	813	37.7	20.9	0.06	5655	0.04978	0.18	0.3659	0.22	0.873	0.0533	0.11	313.2 ± 1.1	316.6 ± 1.2	342 ± 5	8.6
Zrn10b -s, lp, 220 × 110	8	1336	61.7	11.0	0.06	36406	0.05007	0.29	0.3680	0.31	0.965	0.0533	0.09	314.9 ± 1.8	318.2 ± 1.7	342 ± 4	8.2
Rt1 -m, sh, 80 × 60, rb	286	28	1.30	64.6	0.02	894	0.05199	0.19	0.3796	0.37	0.673	0.0530	0.28	326.7 ± 1.2	326.7 ± 2.1	327 ± 13	0.0
LU4 Garnet-rich granulite																	
Zrn6 -s, sp, 300 × 150	7	807	50.1	24.5	0.21	5192	0.06465	0.32	0.4929	0.44	0.861	0.0553	0.23	403.8 ± 2.5	406.9 ± 2.9	424 ± 10	5.0
Zrn7 -m, lp, 180 × 80, cl	4	562	39.9	26.0	0.21	2061	0.07121	0.40	0.5569	0.82	0.673	0.0567	0.62	443.4 ± 3.4	449.5 ± 5.9	480 ± 27	7.8
Zrn8 -m, sp, 130 × 80, cl	5	410	26.0	21.0	0.35	2027	0.06144	0.32	0.4656	0.64	0.788	0.0550	0.43	384.4 ± 2.4	388.2 ± 4.1	410 ± 19	6.6
Zrn9 -m, rm, 80 × 80	12	585	30.6	25.9	0.20	4607	0.05360	0.39	0.4062	0.53	0.806	0.0550	0.32	336.6 ± 2.5	346.1 ± 3.1	411 ± 14	18.5
Rt4 -m, sh, 200–250, rb	226	109	5.23	526	0.02	184	0.05288	0.49	0.3858	1.44	0.767	0.0529	1.11	332.2 ± 3.2	331.3 ± 8.1	325 ± 50	−2.1
LUA2 Cordierite-bearing granite																	
Zrn4 -m, r, 100 × 100, cl	16	680	42.6	84.9	0.19	779	0.06039	0.72	0.4523	1.03	0.847	0.0543	0.57	378.0 ± 5.3	378.9 ± 6.5	384 ± 26	1.7
Zrn4a -m, r, 100 × 100	5	384	22.4	11.2	0.21	6386	0.06049	0.19	0.4535	0.33	0.847	0.0544	0.23	378.6 ± 1.4	379.7 ± 2.0	387 ± 11	2.1
Zrn4b -s, r, 130 × 100, cl	2	1193	105	205	0.20	128	0.05908	0.51	0.4420	2.33	0.648	0.0543	2.04	370.1 ± 3.7	371.6 ± 15	382 ± 91	4.2
Zrn5 -s, lp, 300 × 150, cl	12	384	29.9	41.1	0.18	2041	0.07856	0.53	0.6764	0.75	0.882	0.0624	0.38	487.5 ± 5.0	524.6 ± 6.2	689 ± 16	31
Zrn6 -s, om, 300 × 250	20	376	23.4	85.7	0.12	573	0.06563	1.39	0.5871	2.96	0.848	0.0649	2.16	409.8 ± 2.3	469.0 ± 2.3	770 ± 88	48
Zrn7 -m, lp, 300 × 150, cl	25	544	35.7	87.1	0.16	974	0.06488	0.43	0.5060	0.58	0.881	0.0568	0.29	405.3 ± 3.2	415.7 ± 3.8	483 ± 13	17.3
Zrn8 -m, sp, 180 × 100, cl	34	676	36.8	48.1	0.12	4371	0.05697	0.39	0.4265	0.44	0.971	0.0543	0.11	357.2 ± 2.7	360.7 ± 2.7	384 ± 5	7.1
Mz1 -s, eh, 200 × 80, cl	15	4395	1448	931	18.9	264	0.05275	0.72	0.3840	1.09	0.831	0.0528	0.64	331.4 ± 4.6	330.0 ± 6.2	320 ± 29	−3.7
Mz2 -s, eh, 200 × 80, cl	11	2387	1256	101	32.8	1232	0.05299	0.54	0.3854	0.65	0.911	0.0527	0.27	332.8 ± 3.5	331.0 ± 3.7	318 ± 13	−4.7
Rt1 -m, eh, 100 × 60, br	75	18.3	0.88	18.7	0.04	547	0.05252	0.20	0.3847	1.12	0.539	0.0531	1.03	330.0 ± 1.3	330.5 ± 6.3	334 ± 46	1.3
B2 Durbachite																	
Zrn10 -m, lp, 220 × 100	9	969	51.0	25	0.27	6140	0.05329	0.38	0.3933	0.45	0.933	0.0535	0.17	334.7 ± 2.5	336.8 ± 2.6	351 ± 7	4.9
Zrn11 -m, lp, 200 × 80	11	840	43.4	20.2	0.23	8109	0.05290	0.37	0.3937	0.41	0.892	0.0540	0.19	332.3 ± 2.4	337.0 ± 2.4	370 ± 8	10.4
Zrn12 -m, lp, 250 × 100	18	1368	69.7	24.9	0.25	17099	0.05208	0.34	0.3864	0.35	0.925	0.0538	0.13	327.3 ± 2.0	331.7 ± 2.2	362 ± 6	10.1
Zrn13 -m, eh, 80 × 20	18	1119	51.6	79.5	0.21	1822	0.04787	0.46	0.3518	0.49	0.957	0.0533	0.14	301.4 ± 2.7	306.1 ± 2.6	342 ± 6	12.1
Rt5 -m, ds, 200–160, db	91	11.0	0.52	10.5	< 0.01	1603	0.05237	0.18	0.3840	0.56	0.524	0.0532	0.50	329.1 ± 1.2	330.1 ± 3.2	337 ± 23	2.2

[a]Zrn, zircon, abraded 2–8 h after Krogh (1982); Mz, monazite; Rt, rutile; s, single grain; m, multiple grain fraction; cl, clear; eh, euhedral; sh, subhedral; r, rounded; rm, rounded-multifaceted; lp, long-prismatic; sp, short-prismatic; o, oval; om, oval-multifaceted; db, dark-brown; rb, red-brown; co, composite grain; ds, disc-shaped.
[b]Maximum errors are ±50% for weights < 0.002 mg, and ±20% for weights > 0.002 mg.
[c]Radiogenic Pb.
[d]Common Pb.
[e]Measured ratio corrected for fractionation only; Pb fractionation correction = 0.11%/amu (±0.30%).
[f]Corrected for fractionation, spike, blank and initial common Pb.
[g]Degree of discordance.

The dark cores and relict zoning in some of the metamorphic grains (Fig. 6a,h) suggest incomplete obliteration of the primary texture, whereas rounded (Fig. 6c,h,i) and resorbed (Fig. 6d) shapes with relatively homogeneous internal textures are interpreted as almost complete obliteration of the initial magmatic zonation caused by granulite facies metamorphism (Vavra *et al.*, 1996; Hoskin & Black, 2000).

© 2007 Blackwell Publishing Ltd

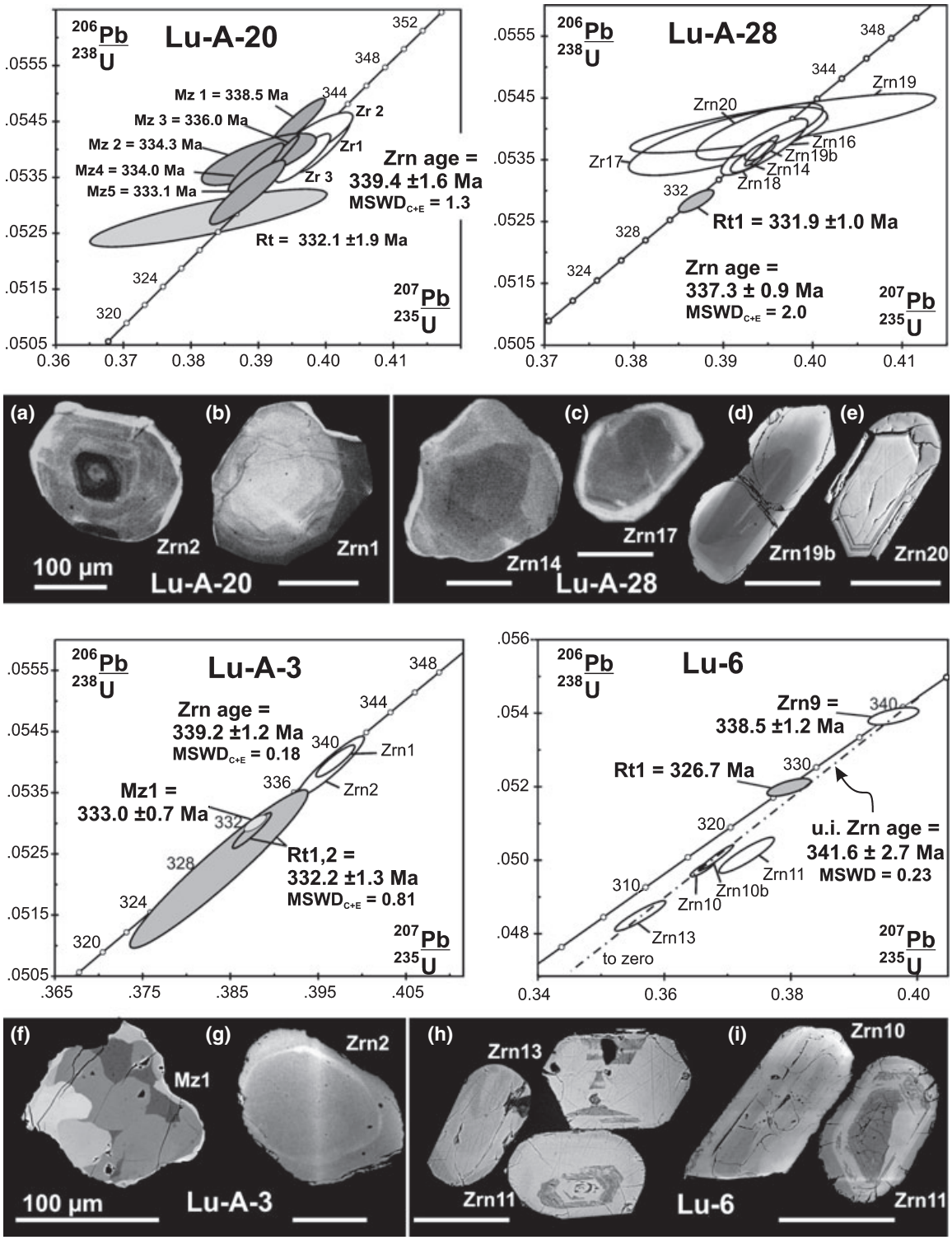


Fig. 6. Concordia diagrams and cathodoluminescence (a,b & c) and back-scattered electron (all other) images of representative zircon and monazite from the analysed samples. Uniform scale is 100 μm. Samples LUA20 and LUA3 contained exclusively spherical zircon grains, typically showing no cores (b & g). Grains which have a relict core and oscillatory zoning preserved are rare (a). A narrow more luminescent (CL) rim can be seen, too. From several zircon types analysed in LUA28 sample, an example of a spherical (c; cf. Zrn14, 16 & 17 in the concordia diagram) and composite and long prismatic zircon type (d & e), with relics of oscillatory zoning and recrystallized rim or overgrowth are shown. Presented monazite from LUA3 (f) is associated with the Crd-Opx-bearing symplectite (Fig. 7a). Rounded multifaceted (cf. Zrn9 in concordia diagram) to short–long prismatic zircon from sample LU6 (h) commonly show relics of oscillatory zoning in the otherwise fully recrystallized grains (h & i).

© 2007 Blackwell Publishing Ltd

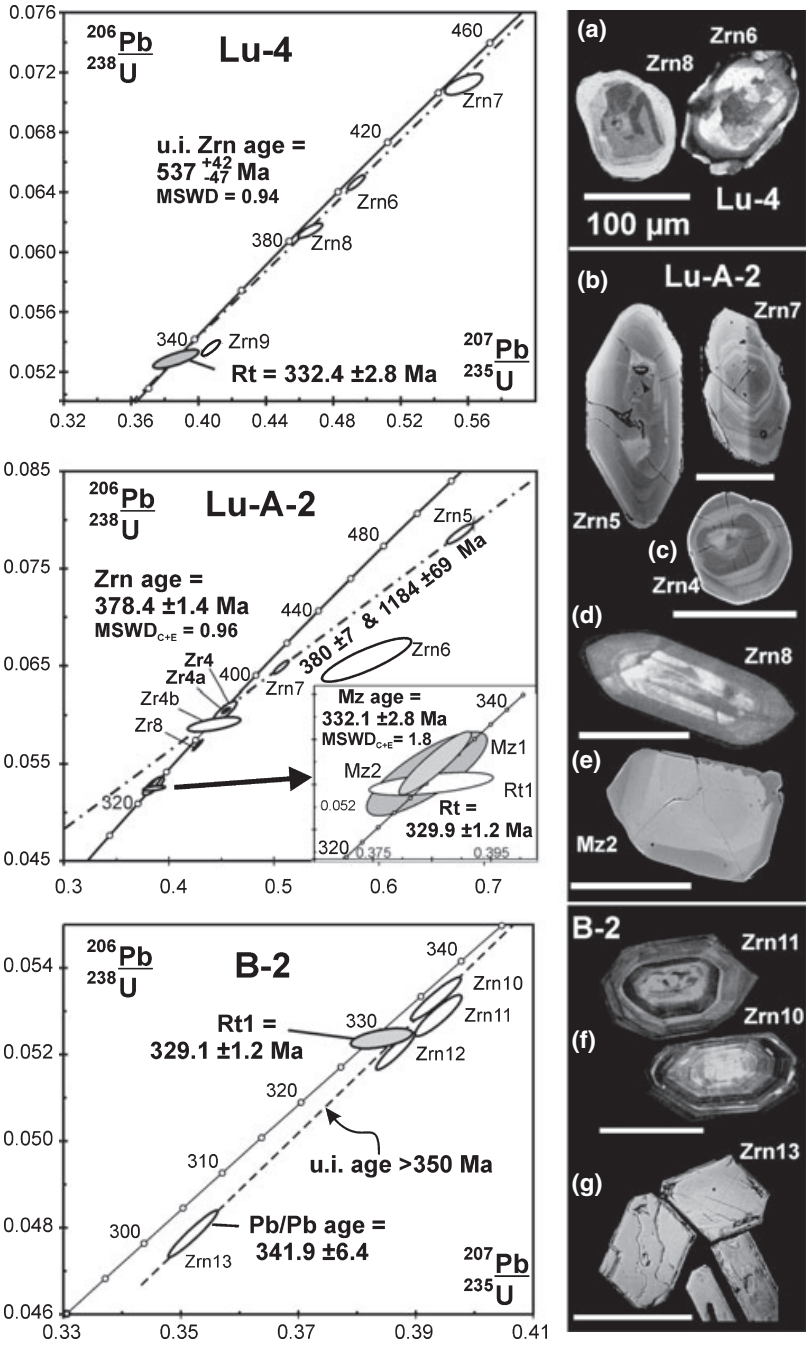


Fig. 7. Concordia diagrams and cathodoluminescence (a, d & f) and back-scattered electron (b, e & g) images of representative zircon and monazite for the analysed samples. Uniform scale is 100 μm. Rounded multifaceted and short prismatic zircon grains from granulite sample LU4 show complex replacement textures with bright luminescent rim (a). Long prismatic zircon with rounded edges (b & d; cf. Zrn5 & Zrn7 in concordia diagram) and spherical zircon (Zrn4, Zrn4a & Zrn 4b) with distinct oscillatory zoning (c), in some cases with recrystallized cores (long prismatic grain) are characteristic of LUA2 granite sample. Euhedral monazite from LUA2 (e) has a dark, probably Th-poor rim with embayments into the core reflecting secondary replacement. B2 durbachite contains mainly long to short prismatic zircon (cf. Zrn10-Zrn12 in concordia diagram) with well-preserved oscillatory zoning. Typical are bright (CL) cores and rims, separated by darker (f) and tabular grains (cf. Zrn13 in concordia diagram) with finer oscillatory zoning in the rim (g).

Both spherical and prismatic zircon from LU4 contains oval cores with a bright, 20- to 40-μm-thick unzoned overgrowth. The cores usually show complex replacement textures in CL (Fig. 7a), while a weak oscillatory zoning is still observable by BSE imaging and optical microscopy.

Cordierite granite (LUA2) and melagranite (B2) are characterized by short to long prismatic, euhedral zircon grains typically with oscillatory zoning, suggesting a magmatic origin. In LUA2, long prismatic grains are generally clear with slightly rounded terminations. The beginning of recrystallization is visible as the primary oscillatory zones are blurred and thickened (Fig. 7b). The grains can either contain darker (BSE) prismatic subrounded inner cores, with relict oscillatory zoning or can be completely recrystallized (Fig. 7b). Still other grains show a bright luminescent inner part surrounded by a dark-grey rim (Fig. 7d) with no evidence of more than one period of magmatic zircon growth. Small (~100–150 μm in diameter) rounded multifaceted zircons make up 10–20% of the LUA2 zircon population. Some show small oscilla-

© 2007 Blackwell Publishing Ltd

tory-zoned cores surrounded by a relatively homogenous grey (BSE) mantle, where the primary oscillatory zoning is almost completely obliterated, and a zoned rim (Fig. 7c).

In melagranite B2, large and clouded prismatic grains dominate over small, even acicular, generally transparent ones and subordinate tabular crystals (Fig. 7f,g). All three types show well-preserved magmatic oscillatory zoning without evidence of a metamorphic overprint, such as rounded edges or recrystallization. Prismatic grains commonly have equant or partly resorbed cores and equant mantles, both with bright luminescence and oscillatory zoning, separated by a dark ~10 μm wide zone, suggesting multiphase zircon-forming processes (Fig. 7f). Tabular (Fig. 7g) and acicular crystals show a homogenous internal texture with fine oscillatory zoning only in the outer part.

Monazite

Monazite has been identified only in three of the rocks studied. Separated monazite grains of the garnet-rich granulite (LUA20) are olive green, clear, generally euhedral to subhedral crystals up to ~250 μm in diameter. They appear homogeneous or slightly patchy under BSE. In the Grt-Crd-Sil-bearing granulite (LUA3), monazite is subhedral, rounded to subrounded or elongate, yellowish and up to 100 μm in diameter/length. It is commonly intergrown with rutile. It features complex internal structure, being composed of irregular patches or rounded subgrains of three to four different shades of grey and a narrow (<10 μm wide) rim under BSE (Fig. 6f), probably differing in Th contents. The zoning can be described as intergrowth-like or sector zoning, being characteristic of monazite from high-grade metamorphic terranes (Bingen & van Breemen, 1998). The monazite grains have commonly light rims under BSE. Euhedral, sub-prismatic and sub-rounded monazite (size up to 200 μm in diameter/length) from cordierite-bearing granite (LUA2) can be cloudy, commonly containing minute dark inclusions. It shows a simple zoning pattern with a light euhedral to subhedral core surrounded by a narrow (up to 20 μm wide) dark rim (Fig. 7e). Dark embayments into the core represent fronts of secondary replacement (Bingen & van Breemen, 1998).

Rutile

Rutile is present in all samples. It forms generally subhedral elongated dark brown (B2, LUA20, LU6 & LUA28) and reddish brown translucent long prismatic (LU4 & LUA2) crystals. Sample LUA3 contains both darker large grains up to 200 μm long and small (up to 120 μm long) reddish brown translucent crystals with more euhedral shape. The latter were selected for the dating.

RESULTS OF U-PB DATING

Analysis of the spherical zircon grains of the different granulites yield comparable U-Pb ages (Figs 6 & 7) that vary from 339.2 ± 1.2 Ma (all uncertainties given as $\pm 2\sigma$) for Grt-Crd-Sil-bearing granulite (LUA3, Zrn1 + 2), 339.4 ± 1.6 Ma for garnet-rich granulite (LUA20, Zrn2 + 3) and 338.5 ± 1.2 Ma for garnet-bearing leucogranulite (LU6, Zrn9) to 337.2 ± 1.2 Ma for Grt-Opx-bearing granulite (LUA28, Zrn14). Oval and composite zircon fractions (Zrn18, Zrn19) of the latter sample give identical U-Pb ages (337 ± 1.5 Ma, MSWD = 0.72). Although most analyses of the four granulite samples appear to plot slightly below concordia, their error ellipses (2σ) overlap in all cases with concordia, taking into account the decay constant uncertainty. The uniform cluster of U-Pb ages around 337 ± 1 Ma in the four different grain fractions of the Grt-Opx-bearing granulite (LUA28) and around 339 ± 1 Ma for the six single spherical grains of the remaining granulite samples suggest no significant effect of Pb-loss and inheritance of older material in these analyses. Therefore, the U-Pb ages can be considered as best estimate for the time of crystallization or recrystallization of spherical and oval zircon in these granulites.

One single-grain and two multi-grain fractions of prismatic zircon grains from LUA28 yield a concordia age of 338.3 ± 1.4 Ma, which is indistinguishable from that of spherical, oval and composite LUA28 grains (337.1 ± 1.1 Ma, MSWD = 1.8). All grains feature similar uranium contents as well.

All prismatic zircon analyses of the leucogranulite (LU6) are discordant, suggesting different degrees of Pb loss. Two single- and one multi-grain fractions define a discordia with intercepts at 353 ± 44 and 96 ± 260 Ma respectively. Anchoring the discordia at zero defines a more precise upper intercept age of 341.6 ± 2.7 Ma (Fig. 6), which is within error indistinguishable from the age of the spherical zircon of 338 ± 1.2 Ma. Another multi-grain fraction (Zrn11) plots below this discordia suggesting the presence of an older, inherited component in addition to lead loss. In contrast to the sample LUA28, the prismatic grains have much higher U contents (800–1300 ppm) than the spherical grains (~180 ppm).

Zircon analyses of biotite-garnet-bearing granulite (LU4) are all discordant with U-Pb ages >340 Ma, suggesting different degrees of inheritance (Fig. 7). One single- and two multi-grain prismatic zircon fractions define a discordia with a lower intercept around 346 Ma. Neither upper nor lower intercept are well defined. Forcing the discordia through 340 Ma results in an upper intercept age of 537 +42/−47 Ma. Small rounded zircons (Zrn9) from this sample falls to the right of this discordia, indicating the presence of an older inherited component.

Three analyses of small rounded zircon from cordierite-bearing granite (LUA2) are concordant to sub-

© 2007 Blackwell Publishing Ltd

concordant with U-Pb ages ranging from 380 to 370 Ma. Only analyses of Zrn4 and Zrn4a can be considered as equivalent (Fig. 7) yielding of concordia age of 378.4 ± 1.4 Ma ($MSWD_{C+E} = 0.96$; C + E = concordance and equivalence). The remaining analysis, Zrn4b, suggests that the zircon suffered from Pb loss. Single- and multi-grain analyses of prismatic zircon show variable discordance. Fractions Zrn5 and Zrn7 define a discordia with upper and lower intercept of 1.184 ± 69 and 379.7 ± 7.0 Ma respectively. The latter is identical to the concordant age of rounded zircon. The $^{207}Pb/^{206}Pb$ age (384 ± 5 Ma) of a discordant multi-grain fraction of small prismatic zircon is also very similar (Zrn8), suggesting, as in case of the small rounded zircon, no or only minor inheritance. An oval zircon (Zrn6) gives the lowest $^{206}Pb/^{238}U$ (*c.* 340 Ma) and highest $^{207}Pb/^{206}Pb$ ages (*c.* 770 Ma), indicating the combined effect of Pb loss and inheritance.

Melagranite B2 zircon grains are U-rich and commonly strongly metamict (clouded prismatic grains). Analyses of prismatic grains are variably discordant (Fig. 7) with $^{206}Pb/^{238}U$ ages around 330 Ma and $^{207}Pb/^{206}Pb$ ages from 370 to 351 Ma, suggesting variable amount of inheritance together with recent Pb loss. Tabular grains (Zrn13) are more discordant, but yield a lower $^{207}Pb/^{206}Pb$ age of 342 ± 6 Ma. A discordia including the analyses of prismatic grains yields poorly defined upper intercept ages of > 350 Ma (Fig. 6).

Monazite

Monazite grains from garnet-rich granulite (LUA20) are reverse-discordant, with $^{206}Pb/^{238}U$ ages of around 1–4 Myr older than the $^{207}Pb/^{235}U$ ages. The degree of discordance roughly correlates with the U/Th and the age, with the oldest (Mz1-2) being −7% to −11% discordant and the youngest monazite Mz5 concordant (−0.6%) within error. There are two common explanations for reverse concordance. One is excess ^{206}Pb caused by the decay of ^{230}Th that is not derived from the decay of ^{238}U in the crystal, and the second is incomplete spike–sample equilibration. From our experience, the conditions were sufficient to achieve equilibration and in all cases dissolution was complete. Therefore the presence of excess ^{206}Pb in LuA20 monazite seems to be likely and the $^{207}Pb/^{235}U$ ages were used for interpretation. The ages range between 338.5 ± 2.5 and 333.1 ± 3.4 Ma (Fig. 6) and just overlap within error with each other. The weighted mean is 335.6 ± 2.7 with a somewhat elevated MSWD of 2.5. This suggests more than one age of monazite growth.

Rounded monazite from the Grt-Crd-Sil-bearing granulite (LUA3; Fig. 6) yielded a concordant result within error. The concordia age of 333.0 ± 0.7 Ma (MSWD = 0.09) overlaps with the lower age range of LUA20 monazite. Euhedral monazite from cordierite-bearing granite (LUA2) is concordant to slightly reverse-discordant (Fig. 7). The weighted mean $^{207}Pb/^{235}U$ age of 330.7 ± 3.1 Ma is indistinguishable from the concordia age of 332.1 ± 2.8 Ma.

Rutile

Rutile has variable U contents between 11 and 110 ppm and commonly high $^{206}Pb/^{204}Pb$ (> 500). Only rutile from LUA2 and LU20 has low $^{206}Pb/^{204}Pb$, which relates to elevated errors in the $^{207}Pb/^{235}U$ age. Nevertheless, all analyses can be interpreted as concordant. The concordia ages (MSWD of concordance generally < 0.8) are around 332 ± 1–3 Ma for rutile from granulite samples, except for rutile from garnet-bearing leucogranulite LU6, which yields a significantly younger age of 327 ± 1 Ma (Fig. 6). Rutile from granite LUA2 (329.9 ± 1.2 Ma) and from melagranite B2 (329.0 ± 1.2 Ma) both give ages around 330 Ma (Fig. 7).

DISCUSSION

Internal structures and age of granulite zircons

Uranium–lead ages of spherical and prismatic zircon grains from several granulite samples fall into a narrow range of 340–337 Ma, indicating a single HT event. Concordancy of the data provides evidence that there are no older age components present – despite some relicts of the primary texture, such as oscillatory zoning or older cores, observed in different grains. The CL images clearly indicate the replacement of primary textures as well as rounding and resorption of grain boundaries. Therefore, the primary age information on an older, possibly magmatic stage was completely obliterated. Alternatively, this event of primary zircon growth happened shortly before the metamorphic overprint and the two events cannot be resolved using zircon chronometry. Prismatic (magmatic) and rounded (metamorphic) zircon grains of LUA28 give identical ages within 1 Myr or less.

Except for sample LU4, the U-Pb data do not show any significant inheritance in spherical zircon. Thus, cores visible on some CL/BSE images were either not present in the analysed zircon, completely reset or not significantly older than multifaceted grains. The presence of inherited cores in both zircon types of biotite-garnet granulite (LU4) as indicated by the BSE is reflected by the discordance of the data. It clearly indicates the presence of an older, probably Neoproterozoic component in this rock of paragneiss-like composition and again an HT event at *c.* 340 Ma as for the other granulites.

Uranium-rich prismatic zircons from leucogranulite sample (LU6), showing relic oscillatory zoning under BSE, yield age identical within error to that of the U-poor spherical ones, which are light-grey and unzoned under BSE. Coarsening or even extinguishing of the original growth zoning of the crystal (Fig. 6h) is

© 2007 Blackwell Publishing Ltd

characteristic of loss of U, commonly coupled with resetting of U-Pb system (Vavra *et al.*, 1996). It is probable that the prismatic grains crystallized in the presence of melt, whereas the spherical ones reflect subsequent sub-solidus or 'metamorphic' zircon growth (Guan *et al.*, 2002) or complete resetting during granulite facies metamorphism. As in the case of LUA28, the prismatic grains in LU6 grew only shortly before 'metamorphic' zircon at *c.* 350–340 Ma. Any significantly older inheritance would be visible in the U-Pb data. Assuming that zircon has grown during the HP event (see subsequent section), such a finding is in line with the interpretation of the HP leucogranulites of the Bohemian Massif as products of dehydration melting under high pressures (Kotková & Harley, 1999) and rapid succession of events during exhumation.

Spherical zircon grains of the more mafic granulites (LUA20, LUA28 & LUA3) rarely preserve a weak oscillatory zoning (Fig. 6a) but mostly they are light grey and unzoned in BSE, which suggests a large extent of zircon recrystallization. They exhibit low Th/U ratios, typical of 'metamorphic' zircon (Rubatto, 2002). Slightly more discordant ages (e.g. Zrn2, LUA20) might reflect the presence of a somewhat older core (Fig. 6a) which has not been completely reset. Some prismatic zircon from LUA28, unzoned or with relict zoning, features higher Th/U values, pointing to their 'magmatic' origin (crystallization in presence of melt). This applies also to the metasedimentary granulite LU4, obviously containing inherited, oscillatory-zoned 'magmatic' cores in zircon. In contrast, the Th/U ratio of the 'metamorphic' grains from LU6 is higher than that of the 'magmatic' grains because of the low U contents. This is in disagreement with the empirically postulated high Th/U (>0.1) for zircon crystallizing in a melt (Ding *et al.*, 2001; Rubatto, 2002).

A later event of zircon growth or recrystallization, which post-dates spherical zircon formation, is indicated by rims observed in some grains (dark in BSE and unzoned). Because of abrasion this is not documented in the presented data.

Depth ($\sim$ pressure) of zircon and monazite formation

There is an on-going debate as to whether the granulite zircon ages, e.g. *c.* 340 Ma in case of the Variscan Europe, date maximum rock burial or the MP overprint (e.g. Roberts & Finger, 1997; Kröner *et al.*, 2000). Geochronological data from high-grade rocks generally correspond to closure temperatures of the U-Pb system in accessory minerals, and they are not easy to interpret in terms of depth reached. In this respect, textural relationships of zircon – and monazite – can provide useful clues.

Electron microprobe studies of the zircon and monazite-bearing granulite samples (LUA20 & LUA3) in thin section and BSE imaging showed the following features:

- Both spherical zircon and monazite occur enclosed in garnet (close to Grs-enriched core as well as rim; Fig. 8a,c), adjacent to garnet (Fig. 8b), in quartz, feldspar or at quartz-feldspar grain boundaries; monazite is commonly attached to rutile.
- The rounded monazite in the Grt-Crd-Sil-bearing granulite (LUA3) is undisputedly associated with cordierite-orthopyroxene symplectite (Fig. 8d); it features complex zoning as described above (Fig. 6f); monazite also forms elongated grains observed in the matrix as well as in cracks in garnet.

Observed textural relationships suggest that the zircon ages of *c.* 339 Ma can be attributed to the estimated peak pressures, which is in line with other studies (e.g. Romer & Rötzler, 2001). Similar U-Pb ages were yielded by zircon enclosed in Grs-rich garnet from HP granulites of the South Bohemian Moldanubicum (Aftalion *et al.*, 1989). Pressures estimated for this rock ($\sim$14 kbar, Vrána, 1989) approach the peak pressures ($\sim$16 kbar) known for Moldanubian granulites (Carswell & O'Brien, 1993). We therefore argue, along with Kröner *et al.* (2000), that zircon crystallization does not have to post-date the pressure peak as suggested by Roberts & Finger (1997), even though new zircon can also be formed on the decompressional path (zircon rims; Friedl *et al.*, 2003).

The presence of monazite in both the HP (garnet) and MP (symplectite) mineral assemblage is in accordance with its multiple growth or growth over a time period as indicated by radiometric data from LUA20. The 'older' $^{207}Pb/^{235}U$ ages suggest earlier monazite growth during and shortly after zircon growth at *c.* 339 Ma. Both LUA20 and LUA3 granulites contain a 'younger' monazite generation with identical age. Their age of *c.* 333 Ma is interpreted as dating crystallization or recrystallization close to their T_C at high temperature (Jung & Mezger, 2001). As monazite is associated with the symplectites around garnet, the young monazite ages probably date the MP (6 ± 1 kbar) stage of the evolution, for which a minimum temperature of 820 °C has been estimated. The complex patchy BSE pattern (Fig. 6f) indicates replacement or recrystallization of LUA3 monazite with resetting of the U-Pb system. Formation of dark, probably Th-rich grain parts and grains rims in case of LUA3 monazite points to a second period of crystal growth (Zhu & O'Nions, 1999), possibly a second thermal event.

Monazite in cordierite-bearing granite LUA2 is within error indistinguishable from the youngest monazite age from granulites. Both monazite and rounded zircon are situated at the grain boundaries (even at 'triple points' among perthitic Kfs, plagioclase and quartz) and at the rim of these minerals. Moreover, they are enclosed in biotite and in the structurally late cordierite intergrown with quartz. Formation of such aggregates is attributed to the reaction of biotite and melt during the final stages of magma emplacement after the decompression of biotite-bearing mag-

© 2007 Blackwell Publishing Ltd

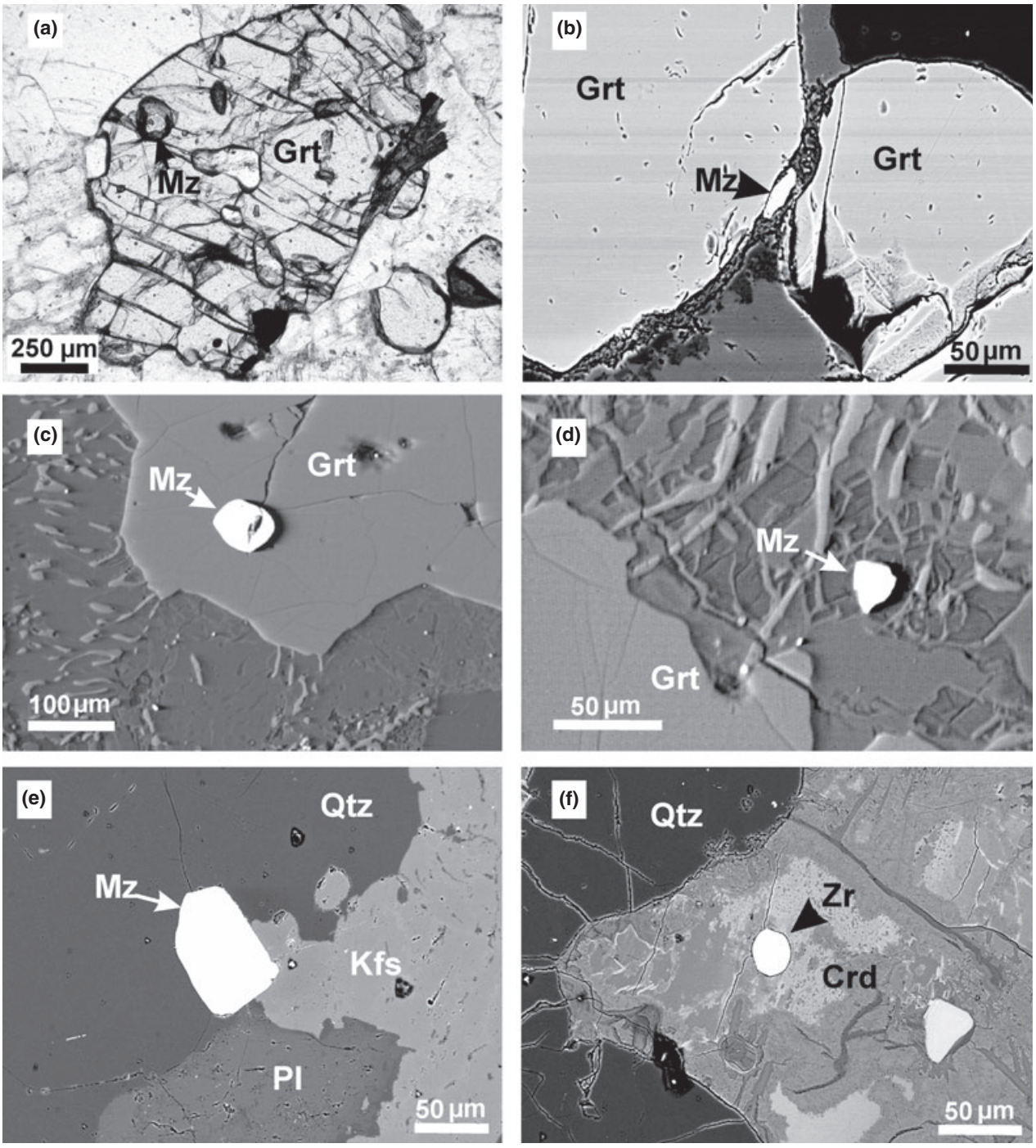


Fig. 8. Photomicrograph (a) and BSE images (b-f) showing position of zircon and monazite in the dated samples. (a) garnet-rich granulite LUA20, monazite within garnet, (b) garnet-rich granulite LUA20 monazite at the garnet rim, (c) Grt-Crd-Sil granulite LUA3, monazite within garnet, (d) Grt-Crd-Sil granulite LUA3, monazite within Crd-Opx symplectite, (e) cordierite granite LUA2, monazite (cf. Fig. 7e) at the grain boundary (f) cordierite granite LUA2, (f) cordierite granite LUA2, zircon (cf. Fig. 7c) within cordierite.

mas equilibrated at depth (cf. the Velay granite, French Massif Central; Barbey *et al*., 1999). The monazite age is interpreted as dating the youngest HT event in this rock, causing formation and crystallization of the restite-rich (as there is a large amount of inherited zircon) cordierite-bearing melt at moderate pressure. The BSE images identify probable low-Th rims on monazite (Fig. 7e) which can reflect secondary replacement (Bingen & van Breemen, 1998), possibly resulting from fluid–mineral interaction in crystallizing

© 2007 Blackwell Publishing Ltd

magma (Hawkins & Bowring, 1997). The overlap between the rutile and the monazite ages, both minerals being closely related (intergrown) in LUA2, indicates rapid cooling to temperatures below 550 °C (Mezger *et al.*, 1989), similar to the granulite samples.

The ages of both spherical and prismatic zircon from LUA2 granite of *c.* 380 Ma are more difficult to interpret, as there is no petrographical evidence about the earlier history of the rock and no field relationships are known. The observed partly recrystallized prismatic cores can represent a 1.2-Ga inherited component. Prismatic shape, presence of oscillatory zoning (Fig. 7b,d) and the textural position of zircon at grain boundaries (Watson *et al.*, 1989) indicate its crystallization in presence of a melt. This suggests that the age of 380 Ma relates to an older melting event, possibly crystallization of the magmatic protolith. Interestingly, zircon of this sample shows no record of the 340 Ma metamorphic event, which dominates the granulite facies rocks. This can mean that the granite was at a higher crustal level where temperature was not high enough for zircon crystallization/resetting.

Discordancy of the data for prismatic zircon of the melagranite sample reflects their complex internal structure (Fig. 7f) and the resulting Pb-Pb age has to be interpreted as a mixed age.

Succession and interpretation of the dated events

Ages similar to the oldest U-Pb zircon age from cordierite-bearing granite (*c.* 380 Ma) are not very common for felsic rocks in the Moldanubian Unit of the European Variscides. In the Bohemian Massif, they were reported for zircon from granulite samples by Wendt *et al.* (1994, leucogranulite, south Bohemia, cores of prismatic grains), Schulmann *et al.* (2005, south Moravia, various zircon types), and interpreted as the intrusion or crystallization age of the granulite precursor. A somewhat younger age of around 370–360 Ma was obtained from prismatic zircon from granodioritic gneiss associated with granulites (Kröner *et al.*, 2000) and from oscillatory zoned prismatic grains from south Bohemian LP granulites (Janoušek *et al.*, 2006).

Some Sm-Nd data for peridotites in the Gföhl Unit yield 380–370 Ma ages in addition to the *c.* 340 Ma ages, which may reflect an older HP event (Medaris *et al.*, 1995). Nevertheless, cordierite granite LUA2 does not preserve any petrological evidence for an HP event.

The U-Pb zircon granulite ages for granulite clasts closely cluster at 339 ± 1 and 337 ± 1 Ma, and fall within the age interval yielded by zircon from the Moldanubian granulites in the Bohemian Massif (van Breemen *et al.*, 1982; Aftalion *et al.*, 1989; Kröner *et al.*, 2000; Schulmann *et al.*, 2005; Janoušek *et al.*, 2006).

The Pb-Pb age of 342 ± 6 Ma for K-Mg-rich melagranite is similar to the Pb-Pb age of 340 ± 8 Ma reported by Holub *et al.* (1997) for the Třebíč melagranitoid massif (Fig. 1a) and close to the U-Pb age of 338 ± 2 Ma for tabular zircon from Rastenberg granodiorite (Klötzli & Parrish, 1996). The upper limit for the melagranite emplacement is represented by the rutile age of *c.* 330 Ma as well as the age of conglomerate sedimentation. The data are within error of well-constrained ages of 337–336 Ma, interpreted as dating the emplacement of ultrapotassic igneous rocks in the middle crust (Janoušek & Gerdes, 2003; Kotková *et al.*, 2003). Such an age is compatible with the emplacement ages of similar ultrapotassic igneous rocks throughout Variscan Europe.

The monazite ages of 333 Ma from the granulites are interpreted to date the HT event, which caused the observed MP overprint of their assemblages (~6 kbar & 820 °C). Similar ages have been reported for granulites (*c.* 333 Ma, SHRIMP, zircon rims) and gneisses of the Gföhl (*c.* 334 Ma, monazite) and Ostrong (*c.* 339 & 334 Ma, monazite) Units in the Lower Austria (Friedl, 1997; Friedl *et al.*, 2003). This thermal event is synchronous or pre-dates the generation of voluminous Moldanubian granites (Weinsberg and Eisgarn group), emplaced as different intrusions at around 331, 328, 326 and 322 Ma (U-Pb ID-TIMS zircon and monazite, Gerdes, 2001; Gerdes *et al.*, 2002). Moreover, monazite data of the cordierite granite (332 ± 3 Ma) suggest a direct link between emplacement of some types of magmas and the younger MP/HT event documented by the granulites and the high-grade gneisses. These data indicate a rather long-lasting period of high heat flow in the Variscan crust of the Bohemian Massif (Gerdes *et al.*, 2000).

TECTONIC SCENARIO

The clast-supported LC of the uppermost part of the Culm sedimentary sequence are restricted to the southern part of the foreland basin. They represent proximal gravity flow sediments, chiefly sub-aquatic slope deposits of the coarse-grained delta system, where the deposition proceeded from the high-density turbidity currents, debris flows and slumps (Nehyba & Mastalerz, 1995). The very low shape anisotropy of the conglomerates indicates a depositional origin of the inner fabric of the conglomerates (Havíř, 1999).

Hartley & Otava (2001) presented a concept of point-source-derived axial system without a tectonic control for the southern part of the Culm basin. In contrast, Bábek *et al.* (2004) found evidence for lateral sediment supply in the northern part of the basin, reflecting increased tectonic activity. And indeed, the age of sedimentation of the LC (330–325 Ma) corresponds to the timing of the collision of the Moldanubian terrane with the Brunovistulicum continental block in the east and the associated nappe stacking. The complex nappe structure at the SE margin of the Bohemian Massif has been interpreted in terms of the polyphase or sequential nappe

© 2007 Blackwell Publishing Ltd

stacking resulting from this oblique collision. In the concept of Schulmann *et al.* (1994), intra-Moldanubian stacking towards the SE brought the high-grade rocks of the Gföhl Unit on top of the Moldanubian nappe sequence. The Moldanubian units were subsequently piled over the Moravian foreland towards the NE, which resulted in stacking of the Moravian nappes between Moldanubicum and Brunovistulicum. In other models, all the exhumation of the Gföhl granulites proceeded in the NE-directed thrusting regime (Urban, 1992; Fritz *et al.*, 1996). Final exhumation and cooling below ~300 °C is dated by similar Ar-Ar muscovite ages for the Moldanubicum and Moravicum of about 330–325 Ma (Matte *et al.*, 1985; Dallmeyer *et al.*, 1992) and is contemporaneous to the above-mentioned collision. However, compressional deformation in the foreland basin lasted until *c.* 320 Ma, as it affected not only Devonian and Lower Carboniferous but also the Viséan to early Namurian sequences (Hartley & Otava, 2001; Bábek *et al.*, 2006).

A minimum average exhumation rate for granulites in pebbles of 2.8–4.3 mm $year^{-1}$ can be calculated assuming that the zircon age of 339 Ma corresponds to the maximum burial, i.e. min. 12 kbar ~44 km for granodioritic crust (16 kbar ~59 km for exposed Moldanubian granulites – Carswell & O'Brien, 1993), and the age of conglomerate sedimentation of 326 ± 2 Ma. The upper and lower limits of sedimentation are defined by the youngest rutile age of 327 Ma and by biostratigraphical constraints, respectively. Using the zircon age of granulite LUA28, the results would be somewhat higher (3.1–5.5 and 4.0–7.3 mm $year^{-1}$, respectively). Combining the *P–T* data with the zircon, monazite and rutile ages (sample LUA20), the cooling rate can be inferred. This is strongly dependent on the assumed closure/crystallization temperatures. For zircon, the T_C of 900 °C (Mezger & Krogstad, 1997) is taken as the minimum approximation. An interval of 750–820 °C is assumed as the temperature for monazite crystallization/closure based on the results of this study and the data of Spear & Parrish (1996). For rutile, T_C of ~550 °C is applied, taking into account larger grain size and rapid cooling compared with those studied by Mezger *et al.* (1989).

In case of this study, not only closure temperatures but also two monazite ages are critical for the assessment of cooling and exhumation rate for the two stages indicated by the *P–T* path. On the *T–t* plot (Fig. 9), the following possibilities are shown (in all cases, zircon ages are related to the maximum pressure estimate).

(a) Considering the zircon age of 339 Ma, a medium pressure overprint at 333 Ma (young monazite, LUA3 & LUA20-Mz5) and a rutile cooling age of *c.* 332.0 Ma (average of LUA20, LUA3, LUA28 & LU4 rutile), contrasting cooling rates of ~11 to 35 °C Myr^{-1} and ~120 to >200 °C Myr^{-1}, respectively, for the considered ranges of T_C are obtained. This is consistent with a two-stage exhumation, as suggested by the *P–T* path.

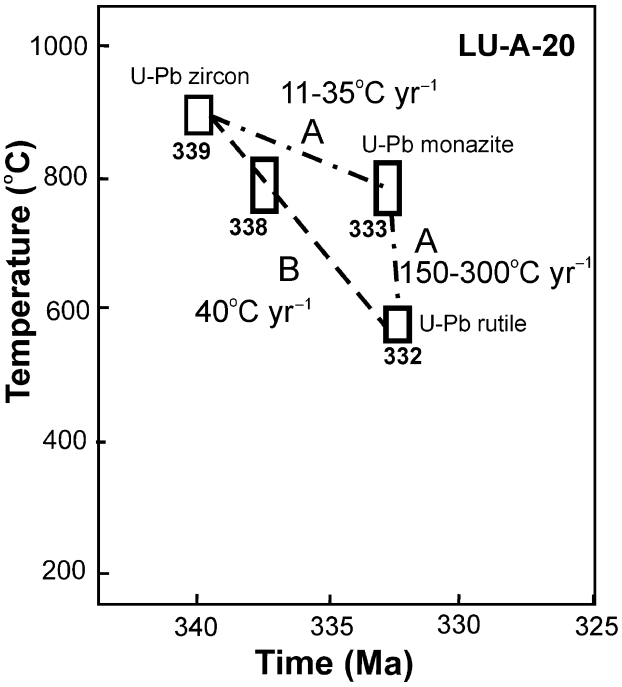


Fig. 9. Temperature–time diagram. (A) medium-pressure overprint at *c.* 333 Ma (young monazite) implies two-stage exhumation with contrasting cooling rate; (B) monazite age of *c* 338 Ma implies constant cooling rate throughout the exhumation.

(b) Considering that the monazite age of *c.* 338 Ma reflects cooling to ~800 °C, a constant cooling rate of ~40 °C Myr^{-1} throughout the exhumation can be calculated, which would be incompatible with a two-stage *P–T* evolution.

As for the exhumation rate of the two stages indicated by the *P–T* path, an exhumation rate of 2.7–4.7 mm $year^{-1}$ for the decompressional stage can be inferred using the young monazite age of 333 Ma for the MP event.

Synorogenic clastic sediments from the upper part of the Variscan foreland basin contain granulites with U-Pb zircon age of *c.* 340 Ma, attributed to the maximum burial of granulites now found in clasts. This, along with the shape of their *P–T* path and the Ar-Ar ages of detrital muscovite from the LC of 341–327 Ma (Schneider *et al.*, 1999), suggests that the source area contained material similar to the Moldanubian (Gföhl) Unit exposed today. However, there are important contrasting features of the LC compared to present denudation level.

1 Melagranites in clasts have a leucocratic character; exotic subvolcanic and volcanic members of the ultrapotassic igneous rock series (Zachovalová & Leichmann, 2004) dated at 346 ± 6 Ma (Ar-Ar biotite; Kotková *et al.*, 2002) are also present.

2 There is no evidence in the LC for the presence of HP granulites, eclogites and garnet peridotites, which are closely associated with each other in the exposed Moldanubian Gföhl Unit; the greywacke matrix, too, is

© 2007 Blackwell Publishing Ltd

dominated by Ca-poor pyrope-almandine garnet (Čopjaková *et al.*, 2001, 2005).

3 Exotic granulites of highly peraluminous bulk-rock composition contain mineral assemblages reflecting an extensive overprint at relatively high temperature of 820 °C at mid-crustal depths.

4 Monazite associated with the HT–MP assemblage was dated at *c.* 333 Ma; contrastingly, SHRIMP zircon ages of *c.* 339 Ma were reported for the HP, MP as well as LP stage of the granulites from the South Bohemian Gföhl Unit (Kröner *et al.*, 2000); 337–335 ± 3 Ma monazite age for LP (2–3 kbar) post-tectonic pegmatites crosscutting the exposed granulite bodies suggest much higher exhumation rate, too, on the order of 16 mm yr^{-1} (Novák, 2001).

Based on these data, we propose that:

1 The clasts were derived from another, structurally higher crustal level than that corresponding to the present day level of denudation of the Moldanubian nappes. This level could have been completely removed by erosion.

2 The intense HT–MP overprint dated at *c.* 333 Ma, which could have erased the earlier higher-pressure (> 12 kbar) history, could reflect prolonged residence of the rocks at mid-crustal levels. This younger HT–MP event is also documented by some zircon and monazite ages for the Moldanubian granulites and Ostrong gneisses (Friedl, 1997; Friedl *et al.*, 2003). The large extent of this overprint documented from the clasts is therefore related rather to a smaller size of the parent bodies than to relatively slow exhumation. Similarly high temperatures characterize the MP overprint on the ultra-HP garnetites from boudins within Gföhl gneisses in the South Bohemian and Moravian Moldanubicum (Kotková *et al.*, 1997; Vrána & Frýda, 2003). This brings about a possibility of a more complex *P–T* evolution of the Moldanubian Gföhl Unit including a thermal pulse on the granulite exhumation path (Kotková *et al.*, 1997; O'Brien, 1997) dated by the present study at *c.* 333 Ma. A more complex exhumation scenario is also suggested by the calculated slow cooling followed by rapid cooling, contrary to what is expected for rapid followed by slow exhumation.

The presence of pebbles and Cr-rich spinels in the greywacke matrix of the LC having equivalents in the lower Moldanubian nappes (Drosendorf Unit) and Moravicum (Olešnice Unit) reflects continuous erosion of the stacked nappe pile. The underlying RC sampled less metamorphosed though deformed rock units of younger age (Cadomian to Early Variscan ages of 590–370 Ma, Ar-Ar detrital muscovite, Schneider *et al.*, 1999), and at their base even the upper part of the crustal sequence, before the Moldanubian nappe stacking.

CONCLUSIONS

Upper Viséan conglomerates in the south-eastern part of the European Variscan foreland basin contain rocks with Moldanubian affinities, which differ, however, in many aspects from those found at the present erosional level.

Spherical zircon grains from different granulite clasts yielded ages of 339.0 ± 0.7 and 337.2 ± 1.1 Ma, interpreted as dating the HP granulite event. Prismatic grains with relict oscillatory zoning yield identical ages within error to those of spherical, completely recrystallized zircon; this is interpreted as formation of 'magmatic' zircon shortly before 'metamorphic' zircon, probably within the same tectono-metamorphic event.

Monazite started to crystallize contemporaneously with the zircon and it may have crystallized continuously over several million years. Nevertheless, the youngest monazite ages from granulites are interpreted as dating the MP–HT overprint on granulites at *c.* 333 Ma at ~6 kbar and 820 °C. At about this time, cordierite-bearing magma (LUA2) was emplaced and rapidly cooled at shallower crustal depths (moderate pressures).

Thermochronology and derived *P–T* path of the granulite pebbles show that they were at first rapidly exhumed along a steep near-to-isothermal decompressional path from at least 44 km to mid-crustal depths of ~22 km. Subsequently, they experienced near-to-isobaric cooling. Granulites were exhumed from deep crust to the surface within 10–12 Myr or less, at a minimum average exhumation rate of 2.8–4.3 mm $year^{-1}$.

We propose that clasts of the LC were derived from a structurally higher crustal level than that presently exposed in the Moldanubicum (presence of exotic volcanic rocks and leucocratic members of the ultrapotassic igneous rock series). The small size of the high-grade rock bodies, exhumed from the lower crustal levels, facilitated the observed HT overprint on the rocks at the mid-crustal depths. The clasts of the underlying RC were derived from the upper part of the crustal sequence and less metamorphosed older units before the Moldanubian nappe stacking.

ACKNOWLEDGEMENTS

This research was sponsored by the grant project of the Czech Grant Agency (GACR 205/99/0567), PACE TMR Network and by the Research No J07/98: 143100004 of the Faculty of Sciences, Masaryk University. Radiometric data were acquired during the research stay of J. Kotková at NIGL, financed by the Europrobe Travel Grant. The study of complex symplectites and acquisition of the EMP data for the *P–T* estimates was carried out using the EU Large Scale Geochemical Facility in Bristol with kind assistance of S. Kearns. A. Gerdes acknowledges financial support of the German Science Foundation (DFG; grant no. GE 1152/1-1). Samples LU4 and LU6 were collected by J. Hladil and provided by S. Vrána. The help of M. Janák with introduction to TWQ technique is grate-

© 2007 Blackwell Publishing Ltd

fully acknowledged, too. The early version of the paper profited from useful comments of U. Schaltegger. Thorough and constructive comments by P. Hoskin and J. Paquette and editorial handling by D. Whitney as well as a language check by S. Chakraborty helped to improve the manuscript and are gratefully acknowledged.

REFERENCES

Aftalion, M., Bowes, D. R. & Vrána, S., 1989. Early Carboniferous U-Pb zircon age for garnetiferous perpotassic granulites, Blanský les massif, Czechoslovakia. *Neues Jahrbuch für Mineralogie-Monatshefte*, **4,** 145–152.

Bábek, O., Mikuláš, R., Zapletal, J. & Lhotský, T., 2004. Combined tectonic-sediment supply-driven cycles in a Lower Carboniferous deep-marine foreland basin, Moravice Formation, Czech Republic. *International Journal of Earth Science*, **93,** 241–261.

Bábek, O., Tomek, C., Melichar, R., Kalvoda, J. & Otava, J., 2006. Structure of unmetamorphosed Variscan tectonic units of the souther Moravo-Silesian zone, Bohemian Massif: a review. *Neues Jahrbuch für Geologie und Paläontologie, Abhandlungen*, **239,** 37–75.

Barbey, P., Marignac, C., Montel, J. M., Macaudiere, J., Gasquet, D. & Jabbori, J., 1999. Cordierite growth textures and the conditions of genesis and emplacement of crustal granitic magmas: the Velay granite complex (Massif Central, France). *Journal of Petrology*, **40,** 1425–1441.

Berman, R. G., 1991. Thermobarometry using multi-equilibrium calculations: a new technique, with petrological applications. *Canadian Mineralogist*, **29,** 833–855.

Berman, R. G. & Aranovich, L. Ya., 1996. Optimized standard state and solution properties of minerals I. Model calibration for olivine, orthopyroxene, cordierite, garnet, and ilmenite in the system FeO-MgO-CaO-Al_2O_3-TiO_2-SiO_2. *Contributions to Mineralogy and Petrology*, **126,** 1–24.

Bingen, B. & van Breemen, O., 1998. U-Pb monazite ages in amphibolite- to granulite-facies orthogneiss reflect hydrous mineral breakdown reactions: Sveconorwegian Province of SW Norway. *Contributions to Mineralogy and Petrology*, **132,** 336–353.

Bohlen, S. R., Wall, V. J. & Boettcher, A. L., 1983. Geobarometry in granulites. In: *Kinetics and Equilibrium in Mineral Reaction* (ed. Saxena, S.K.), pp. 141–171. Springer-Verlag, New York.

van Breemen, O., Aftalion, M., Bowes, D. R. *et al.*, 1982. Geochronological studies of the Bohemian Massif, Czechoslovakia, and their significance in the evolution of central Europe. *Transactions of the Royal Society of Edinburgh, Earth Science Series*, **73,** 89–108.

Buriánek, D. & Novák, M., 2002. Contribution to the knowledge of provenance of pebbles from the Upper Viséan conglomerates in the Drahany Hights: III. Orbicular tourmaline-bearing granite (in Czech with English summary). *Acta Musei Moraviae, Scientiae Geologicae*, **87,** 145–152.

Carswell, D.A. & O'Brien, P.J., 1993. Thermobarometry and geotectonic significance of high-pressure granulites: examples from the Moldanubian Zone of the Bohemian Massif in Lower Austria. *Journal of Petrology*, **34,** 427–459.

Čopjaková, R. & Novák, M., 2003. Contribution to knowledge of provenance of pebbles from the Upper Viséan conglomerates in the Drahany Uplands: IV. Garnet-bearing micaschist with tourmaline (in Czech with English summary). *Acta Musei Moraviae, Scientiae Geologicae*, **88,** 167–175.

Čopjaková, R. & Novák, M., 2005. Provenance changes as reflected in the psephitic and psammitic fraction of the Myslejovice Formation sediments (in Czech). Abstract. Moravsko-slezské paleozoikum, sborník abstraktů, Olomouc, 7–8.

Čopjaková, R., Sulovský, P. & Otava, J., 2001. Use of detrital garnet geochemistry for determination of provenance and lithostratigraphy of the Drahany Upland Kulm. *Mineralia Slovaca*, **33,** 509–511.

Čopjaková, R., Sulovský, P. & Peterson, B., 2005. Major and trace elements in pyrope-almandine garnets as sediment provenance indicators of the Lower Carboniferous Culm sediments, Drahany Uplands, Bohemian Massif. *Lithos*, **82,** 51–70.

Corfu, F., Hanchar, J. M., Hoskin, P. W. O. & Kinny, P., 2003. Atlas of zircon textures. In: *Zircon* (eds Hanchar, J. M. & Hoskin, P. W. O.), *Reviews in Mineralogy & Geochemistry*, **53,** 468–500.

Dallmeyer, R. D., Neubauer, F. & Höck, V., 1992. Chronology of late Palaeozoic tectonothermal activity in the southeastern Bohemian Massif, Austria (Moldanubian and Moravo-Silesian zones): $^{40}Ar/^{39}Ar$ mineral age controls. *Tectonophysics*, **210,** 135–153.

Dallmeyer, R. D., Franke, W. & Weber, K., 1995. *Pre-Permian Geology of Central and Eastern Europe. VIII Moravo-Silesian Zone*. Springer-Verlag, Berlin, Heidelberg, New York, pp. 469–490.

Ding, L., Zhong, D. L., Yin, A., Kapp, P. & Harrison, T. M., 2001. Cenozoic structural and metamorphic evolution of the eastern Himalayan syntaxis (Namche Barwa). *Earth and Planetary Science Letters*, **192,** 423–438.

Franke, W., 1995. Rhenohercynian foldbelt; autochthon and non-metamorphic nappe units: stratigraphy. In: *Pre-Permian Geology of Central and Eastern Europe* (eds Dallmeyer, R. D., Franke, W. & Weber, K.), pp. 33–49. Springer-Verlag, Berlin, Heidelberg, New York.

Friedl, G., 1997. *U/Pb Datierungen an Zirkonen und Monaziten aus Gesteinen vom Österrechischen Anteil der Böhmischen Masse*. Doktoral Thesis. Paris-Lodron Universität, Salzburg, Austria.

Friedl, G., Cooke, R. A., Finger, F., McNaughton, N. J. & Fletcher, I. R., 2003. U-Pb SHRIMP dating and trace element investigations on multiple zoned zircons from a South-Bohemian granulite. *Journal of the Czech Geological Society*, **48,** 51.

Fritz, H., Dallmeyer, R. D. & Neubauer, F., 1996. Thick-skinned versus thin-skinned thrusting: rheology-controlled thrust propagation in the Variscan collisional belt (the southeastern Bohemian Massif, Czech Republic-Austria). *Tectonics*, **15,** 1389–1413.

Fuhrman, M. L. & Lindsley, D. H., 1988. Ternary-feldspar modeling and thermometry. *American Mineralogist*, **73,** 201–215.

Gerdes, A., 2001. Magma homogenisation during anatexis, ascent and/or emplacement? Constraints from the Variscan Weinsberg Granites. *Terra Nova*, **13/4,** 305–312.

Gerdes, A., Wörner, G. & Henk, A., 2000. Post-collisional granite generation and HT-LP metamorphism by radiogenic heating: the example from the Varsican South Bohemian Batholith. *Journal of the Geological Society London*, **157,** 577–587.

Gerdes, A., Friedl, G., Parrish, R. R., von Quadt, A. & Finger, F., 2002. U-Pb dating of South Bohemian granites: constraints for the longevity of melting Cadomian crust. Pangeo Austria Abstracts, 56–57.

Gradstein, F. M. & Ogg, J., 1996. A Phanerozoic time scale. *Episodes*, **19,** 3–5.

Green, D. H. & Lambert, I. B., 1965. Experimental crystallization of anhydrous granite at high pressures and temperatures. *Journal of Geophysical Research*, **70,** 5259–5268.

Green, D. H. & Ringwood, A. E., 1967. An experimental investigation of gabbro to eclogite transformation and its petrological applications. *Geochimica et Cosmochimica Acta*, **31,** 767–833.

Guan, H., Sun, M., Wilde, S. A., Zhou, X. H. & Zhai, M. G., 2002. SHRIMP U-Pb zircon geochronology of the Fuping

© 2007 Blackwell Publishing Ltd

Complex: implications for formation and assembly of the North China Craton. *Precambrian Research*, **113,** 1–18.
Harley, S. L., 1984a. The solubility of alumina in orthopyroxene coexisting with garnet in FeO-MgO-Al_20_3-SiO_2 and CaO-FeO-MgO-Al_20_3-SiO_2. *Journal of Petrology*, **25,** 665–696.
Harley, S. L., 1984b. An experimental study of the partitioning of Fe and Mg between garnet and orthopyroxene. *Contributions to Mineralogy and Petrology*, **86,** 359–373.
Hartley, A. J. & Otava, J., 2001. Sediment provenance and dispersal in a deep marine foreland basin: the Lower Carboniferous Culm Basin, Czech Republic. *Journal of the Geological Society of London*, **158,** 137–150.
Havíř, J., 1999. The fabric of the Culm conglomerates in the eastern parts of the Nízký Jeseník and Drahany Uplands, eastern margin of the Bohemian Massif, the Czech Republic. *Geologica Sudetica*, **32,** 1–11.
Hawkins, D. P. & Bowring, S. A., 1997. U-Pb systematics of monazite and xenotime: case studies from the Paleoproterozoic of the Grand Canyon, Arizona. *Contributions to Mineralogy and Petrology*, **127,** 87–103.
Holland, T. J. B., 1980. The reaction albite = jadeite + quartz determined experimentally in the range 600–1200 °C. *American Mineralogist*, **65,** 129–134.
Holub, F. V., 1997. Ultrapotassic plutonic rocks of the durbachite series in the Bohemian Massif: petrology, geochemistry and petrogenetic interpretation. *Sborník Geologických Věd, Ložiskova Geologie Mineralogie*, **31,** 5–26.
Holub, F. V., Cocherie, A. & Rossi, P., 1997. Radiometric dating of granitic rocks from the Central Bohemian Plutonic Complex (Czech Republic): constraints on the chronology of thermal and tectonic events along the Moldanubian-Barrandian boundary. *Comptes Rendus de l'Academie des Sciences, Serie I Fascicule A- Sciences de la Terre et des Planetes*, **325,** 19–26.
Hoskin, P. W. O. & Black, L. P., 2000. Metamorphic zircon formation by solid-state recrystallization of protolith igneous zircon. *Journal of Metamorphic Geology*, **18,** 423–439.
Houzar, S. & Novák, M., 2001. Contribution to knowledge of provenance of pebbles from the Upper Viséan conglomerates in the Drahany Uplands: I. Graphitic quartzite with vanadium-bearing muscovite (in Czech with English summary). *Acta Musei Moraviae, Scientiae Geologicae*, **86,** 103–109.
Houzar, S. & Novák, M., 2002. Contribution to knowledge of provenance of pebbles from the Upper Viséan conglomerates in the Drahany Uplands: II. Calcitic marbles. (in Czech with English summary). *Acta Musei Moraviae, Scientiae Geologicae*, **87,** 137–144.
Janoušek, V. & Gerdes, A., 2003. Timing the magmatic activity within the Central Bohemian Pluton, Czech Republic: geochronology of the Sázava and Tábor intrusions and their geotectonic significance. *Journal of the Czech Geological Society*, **48,** 70–71.
Janoušek, V., Gerdes, A., Vrana, S. *et al*., 2006. Low-pressure granulites of the Lišov Massif, Southern Bohemia: Viséan metamorphism of Late Devonian plutonic arc rocks. *Journal of Petrology*, **47,** 705–745.
Jung, S. & Mezger, K., 2001. Geochronology in migmatites – a Sm-Nd, U-Pb and Rb-Sr study from the Proterozoic Damara belt (Namibia): implications for polyphase development of migmatites in high-grade terranes. *Journal of Metamorphic Geology*, **19,** 77–97.
Klötzli, U. S. & Parrish, R. R., 1996. Zircon U/Pb and Pb/Pb geochronology of the Rastenberg granodiorite, South Bohemian Massif, Austria. *Mineralogy and Petrology*, **58,** 197–214.
Kotková, J., 1998a. Garnet-bearing mafic granulites from the Lišov granulite massif. *Geolines*, **6,** 37.
Kotková, J., 1998b. *Pyroxene-garnet-bearing granulites from the Lišov granulite massif*. MS, Czech Geological Survey, 24 p. (in Czech).
Kotková, J. & Harley, S. L., 1999. Formation and evolution of HP leucogranulites: experimental constraints and unresolved issues. *Physics and Chemistry of the Earth Part A-Solid Earth and Geodesy*, **24,** 299–304.
Kotková, J., Kröner, A., Todt, W. & Fiala, J., 1996. Lower Carboniferous high-pressure event in the Bohemian Massif: evidence from North Bohemian granulites. *Geologische Rundschau*, **85,** 154–161.
Kotková, J., Harley, S. L. & Fišera, M., 1997. A vestige of very high - pressure (ca. 28 kbar) metamorphism in the Variscan Bohemian Massif, Czech Republic. *European Journal of Mineralogy*, **9,** 1017–1033.
Kotková, J., Novák, M., Leichmann, J. & Houzar, S., 2001. Nature and provenance of exotic rock types from Lower Carboniferous Conglomerates (Eastern Bohemian Massif). *Geolines*, **13,** 81–82.
Kotková, J., Leichmann, J. & Novák, M., 2002. HT rocks from the Viséan conglomerates – further evidence for an external heat source in the internal zone of European Variscides. IMA Abstracts, Edinburgh.
Kotková, J., Schaltegger, U. & Leichmann, J., 2003. 338–335 Ma old intrusions in the E Bohemian Massif – a relic of the orogen-wide durbachitic magmatism in European Variscides. *Journal of the Czech Geological Society*, **48,** 80–81.
Kretz, R., 1983. Symbols for rock-forming minerals. *American Mineralogist*, **68,** 277–279.
Krogh, T. E., 1982. Improved accuracy of U-Pb ages by the creation of more concordant systems using an air abrasion technique. *Geochimica et Cosmochimica Acta*, **46,** 637–649.
Kröner, A., O'Brien, P. J., Nemchin, A. A. & Pidgeon, R. T., 2000. Zircon ages for high pressure granulites from South Bohemia, Czech Republic, and their connection to Carboniferous high temperature processes. *Contributions to Mineralogy and Petrology*, **138,** 127–142.
Kumpera, O., 1977. A review of the fauna of the Moravo-Silesian Kulm. In: *Proceedings of the Symposium of Carboniferous Stratigraphy* (eds Wagner, R. H. & Holub, V. H.), pp. 235–264. UUG, Praha.
Kumpera, O. & Lang, V., 1975. Goniatites of the Drahany Culm (Bohemian Massif, Moravo-Silesian Zone) (in Czech). *Časopis slezského muzea, Ser A*, **24,** 11–34.
Ludwig, K. R., 1989. Pb.Dat: a computer program for processing raw Pb-U-Th isotope data. US Geological Survey Open File Report, **88,** 557.
Ludwig, K. R., 2001. *User's manual for Isoplot/Ex Version 2.49, A Geochronological Toolkit for Microsoft Excel*. Berkley Geochronology Center, Special Publication 1a, Berkley, CA.
Matte, P., Maluski, H. & Echtler, H., 1985. Variscan eastward ductile shearing in the Waldviertel Nappes (South Eastern Bohemian Massif, Austria). *Comptes Rendus des Sciences, Serie II*, **301,** 721–729.
Matte, P., Maluski, H., Rajlich, P. & Franke, W., 1990. Terrane boundaries in the Bohemian Massif: result of large-scale Variscan shearing. *Tectonophysics*, **177,** 151–170.
Medaris, L. G., Beard, B. L., Johnson, C. M. *et al*., 1995. Garnet pyroxenite and eclogite in the Bohemian Massif – geochemical evidence for Variscan recycling of subducted lithosphere. *Geologische Rundschau*, **84,** 489–505.
Melichar, R., Kotková, J., 2003. Introduction to regional geology of the eastern margin of the Bohemian Massif. In: *Geology without Frontiers: Magmatic and Metamorphic Evolution of Central European Variscides* (ed. Kotková, J.), pp. 5–10. Excursion Guide, Czech Geological Society, Prague.
Menning, M., Weyer, D., Drozdzewski, G., van Ameron, H. W. J. & Wendt, I., 2000. A Carboniferous time scale 2000: discussion and use of geological parameters as time indicators from Central and Western Europe. *Geologische Jahrbuch*, **A156,** 3–44.
Mezger, K. & Krogstad, E. J., 1997. Interpretation of discordant U-Pb zircon ages: an evaluation. *Journal of Metamorphic Geology*, **15,** 127–140.
Mezger, K., Hanson, G.N. & Bohlen, S.R., 1989. High-precision U-Pb ages of metamorphic rutile - application to the cooling

© 2007 Blackwell Publishing Ltd

history of high-grade terranes. *Earth and Planetary Science Letters*, **96,** 106–118.
Nehyba, S. & Mastalerz, K., 1995. Sedimentological contribution to the study of the Račice and Luleč conglomerates (in Czech). Geologické výzkumy na Moravě a ve Slezsku v r. 1994, 66–68.
Newton, R. C. & Haselton, H. T., 1981. Thermodynamics of the garnet-plagioclase-Al_2SiO_5-quartz geobarometer. In: *Thermodynamics of Minerals and Melts*. (eds Newton, R. C., Navrotsky, A. & Wood, B. J.), pp. 131–147. Springer-Verlag, New York.
Newton, R. C. & Perkins, D., 1982. Thermodynamic calibration of geobarometers based on the assemblages garnet-plagioclase-orthopyroxene (clinopyroxene)-quartz. *American Mineralogist*, **67,** 203–222.
Noble, S. R., Tucker, R. D. & Pharaoh, T. C., 1993. Lower Palaeozoic and Precambrian igneous rocks from eastern England, and their bearing on late Ordovician closure of the Tornquist Sea: constraints from U-Pb and Nd isotopes. *Geological Magazine*, **130,** 835–846.
Novák, M, 2001. Are granitic pegmatites a toy for descriptive mineralogists or a useful tool for geologists? MinPet2001 Symposium. *Mitteilungen der Österreichischen Mineralogischen Gesellschaft*, **146,** 217–219.
O'Brien, P.J., 1997. Garnet zoning and reaction textures in overprinted eclogites, Bohemian Massif, European Variscides: a record of their thermal history during exhumation. *Lithos*, **41,** 119–133.
O'Brien, P. J. & Rötzler, J., 2003. High-pressure granulites: formation, recovery of peak conditions and implications for tectonics. *Journal of Metamorphic Geology*, **21,** 3–20.
O'Hara, M. J., Richardson, S. W. & Wilson, G., 1971. Garnet-peridotite stability and occurrence in crust and mantle. *Contributions to Mineralogy and Petrology*, **32,** 48–68.
Otava, J. & Gilíková, H., 1999. Correlation of lithological markers within the Moravian-Silesian Culm. *Geolines*, **8,** 53–55.
Parrish, R. R., 1987. An improved micro-capsule for zircon dissolution in U-Pb geochronology. *Chemical Geology*, **66,** 99–102.
Pidgeon, R. T., 1992. Recrystallization of oscillatory zoned zircon - some geochronological and petrological implications. *Contributions to Mineralogy and Petrology*, **110,** 463–472.
Pin, C. & Vielzeuf, D., 1983. Granulites and related rocks in Variscan Median Europe: a dualistic interpretation. *Tectonophysics*, **93,** 47–74.
Roberts, M. P. & Finger, F., 1997. Do U-Pb zircon ages from granulites reflect peak metamorphic conditions? *Geology*, **25,** 319–322.
Roddick, J. C., 1987. Generalized numerical error analyses with applications to geochronology and thermodynamics. *Geochimica et Cosmochimica Acta*, **51,** 2129–2135.
Romer, R. L. & Rötzler, J., 2001. P-T-t evolution of ultrahigh-temperature granulites from the Saxon Granulite Massif, Germany. Part II: Geochronology. *Journal of Petrology*, **42,** 2015–2032.
Rubatto, D., 2002. Zircon trace element geochemistry: partitioning with garnet and the link between U-Pb ages and metamorphism. *Chemical Geology*, **184,** 123–138.
Schneider, D., Handler, R., Neubauer, F., Kalvoda, J. & Tomek, Č., 1999. Ar-Ar single and multi-grain ages of detrital white mica from the Silesian Culm basin (Czech Republic). *Geolines*, **8,** 59–60.
Schulmann, K., Melka, R., Lobkowicz, M., Ledru, P., Lardeaux, J.-M. & Autran, A., 1994. Contrasting styles of deformation during progressive nappe stacking at the southeastern margin of the Bohemain Massif (Thaya dome). *Journal of Structural Geology*, **16,** 355–370.
Schulmann, K., Kröner, A., Hegner, E. *et al.*, 2005. Chronological constraints on the pre-orogenic history of deep-seated rocks along the eastern margin of the Variscan orogen, Bohemian Massif, Czech Republic. *American Journal of Sciences*, **305,** 407–448.
Špaček, P. & Kalvoda, J., 2000. Reconstruction of syn- and postsedimentary tectonic events in flysch basin from limestone pebbles variation: Drahany Kulm of the Moravian Rhenohercynian Zone Vol 51, pg 41, 2000. *Geologica Carpathica*, **51,** 37–47.
Spear, F.S., 1993. *Metamorphic phase equilibria and pressure-temperature-time paths*. Mineralogical Society of America, Washington, D.C., MI, 779 p.
Spear, F. S. & Parrish, R. R., 1996. Petrology and cooling rates of the Valhalla complex, British Columbia, Canada. *Journal of Petrology*, **37,** 733–765.
Stacey, J. S. & Kramers, J. D., 1975. Approximation of terrestrial lead isotope evolution by a two-stage model. *Earth and Planetary Science Letters*, **26,** 207–221.
Štelcl, J., 1960. Petrography of Culm conglomerates of the souther part of the Drahany Upland (in Czech). *Folia Universitatis Purkynianae Brunensis, Geologia*, **1,** 1–103.
Tollmann, A., 1982. Grossraumiger variszischer Deckenbau im Moldanubikum und neue Gedanken zum Variszikum Europas. *Geotektonische Forschungen*, **64,** 1–91.
Urban, M., 1992. Kinematics of the Variscan thrusting in the Eastern Moldanubicum (Bohemian Massif, Czechoslovakia): evidence from the Náměšť granulite massif. *Tectonophysics*, **201,** 371–391.
Vavra, G., Gebauer, D., Schmid, R. & Compston, W., 1996. Multiple zircon growth and recrystallization during polyphase Late Carboniferous to Triassic metamorphism in granulites of the Ivrea Zone (Southern Alps): an ion microprobe (SHRIMP) study. *Contributions to Mineralogy and Petrology*, **122,** 337–358.
Vrána, S., 1989. Perpotassic granulites from southern Bohemia – a new rock type derived from partial melting of crustal rocks under upper mantle conditions. *Contributions to Mineralogy and Petrology*, **103,** 510–522.
Vrána, S., 1992. The Moldanubian Zone in southern Bohemia: polyphase evolution of imbricated crustal and upper mantle segments. In: *Proceedings of the 1st International Conference on the Bohemian Massif* (ed. Kukal, Z.), 26 September to 3 October 1988, pp. 331–335. Prague, Czech Republic.
Vrána, S. & Frýda, J., 2003. Ultrahigh-pressure grossular-rich garnetite from the Moldanubian Zone, Czech Republic. *European Journal of Mineralogy*, **15,** 43–54.
Vrána, S. & Novák, M., 2000. Petrology and geochemistry of granulite clasts in the Viséan Luleč conglomerate, Kulm in central Moravia, Czech Republic. *Věstník Českého geologického ústavu*, **75,** 405–413.
Watson, E.B., Vicenzi, E.P. & Rapp, R.P., 1989. Inclusion Host Relations Involving Accessory Minerals in High- Grade Metamorphic and Anatectic Rocks. *Contributions to Mineralogy and Petrology*, **101,** 220–231.
Wendt, J. I., Kröner, A., Fiala, J. & Todt, W., 1994. U-Pb zircon and Sm-Nd dating of Moldanubian HP/HT granulites from South Bohemia. *Journal of the Geological Society of London*, **151,** 83–90.
York, D., 1969. Least squares fitting of a straight line with correlated errors. *Earth and Planetary Science Letters*, **5,** 320–324.
Zachovalová, K. & Leichmann, J., 2004. Contribution to knowledge of provenance of pebbles from the Upper Viséan conglomerates in the Drahany Uplands: V. Durbachites (in sCzech with English summary). *Acta Musei Moraviae, Scientiae Geologicae*, **89,** 161–171.
Zhu, X. K. & O'Nions, R. K., 1999. Zonation of monazite in metamorphic rocks and its implications for high temperature thermochronology: a case study from the Lewisian terrain. *Earth and Planetary Science Letters*, **171,** 209–220.

Received 8 July 2006; revision accepted 10 June 2007.

© 2007 Blackwell Publishing Ltd